STUDIES OF THE EXTERNAL BEAM OF THE McGILL SYNCHRO-CYCLOTRON

by

John W. Hunt, M.Sc.

A Thesis

Submitted to

the Faculty of Graduate Studies and Research

McGill University

in Partial Fulfilment

of the Requirements for the Degree

of Doctor of Philosophy

Radiation Laboratory
Department of Physics

October, 1955

ABSTRACT

This thesis describes the manner in which a beam of 25 x 10^6 protons/second at 90 Mev was extracted from the McGill synchro-cyclotron and taken to a well-shielded position.

A 1.46 gms/cm^2 uranium foil scattered the main cyclotron beam 5.5° into a magnet channel which was placed 3.4° in azimuth from the target and aligned by the current-carrying stretched wire technique. The channel is interrupted to insert iron wedges on the moveable internal probe and thus to adjust for suitable focus of the beam in the vertical plane.

The extracted beam, normally of 6 x 10^{-11} amperes, passes through a vacuum pipe to a specially constructed magnet which bends it through 44° and directs it through an existing eleven foot wall into a corridor.

The 30 μs beam pulses have a maximum energy spread of about 4.5 Mev. The intensity is already higher than can be employed with crystal counters, but a suitable sink for the beam must be provided in order to reduce the present high background.

ACKNOWLEDGEMENTS

Particular thanks are due to my research director, Professor J. S. Foster, for his constant advice and encouragement. He saw the way to take the external beam through an existing wall and thus obtain excellent shielding without disturbing other experiments.

I should like also to thank Mr. W. J. Link for his able and tireless help during the final year of the project.

Thanks are due to Dr. J. S. Kirkaldy and Dr. H. J. Moody for much assistance on the magnet channel and the shimming of the cyclotron magnet respectively. Essential mechanical work has been carried out promptly by the Shop under Mr. S. Doig.

Many graduate students have been very helpful on numerous occasions and on short notice.

Finally, I wish to acknowledge with thanks the award of two Studentships from the National Research Council.

TABLE OF CONTENTS

TABLE OF CONTENTS

Fig. No.	List of Figures	Page No.
Fig.1.	McGill External-Beam Extraction System.	8a
Fig.2.	Glass Plate Studies of Internal Cyclotron Beam.	10a
Fig.3.	Radial Oscillation Amplitude of Internal Beam.	10b
Fig.4.	Channel Location Parameters.	11
Fig.5.	Variation of Extraction Efficiency with Target Thickness.	13a
Fig.6.	Variation of Extraction Efficiency with Angle of Azimuth.	13a
Fig.7.	Ray Tracing Explanation Diagram.	15
Fig.8.	Ray Tracing Plot for Beam Extraction.	16a
Fig.9.	Initial Beam Extraction Installation.	18a
Fig.10.	Magnetic Field Deficit Before Shimming.	18b
Fig.11.	Magnetic Field Contours After Shimming.	19a
Fig.12.	Details of Scattering Target Assembly.	19b
Fig.13.	Ion Source Box Extension.	20a
Fig.14.	D.C. Amplifier and Current Integrator.	21a
Fig.15.	Faraday Cup.	25a
Fig.16.	Variation of External Beam with Cyclotron Magnet Current.	27a
Fig.17.	Internal Focusing of Scattered Beam.	30a
Fig.18.	Focusing of External Beam.	31a
Fig.19.	Details of Magnetic Channel and Focusing Wedges.	33a
Fig.20.	External Proton Beam Profiles.	36a
Fig.21.	Double Focusing Deflection Magnet.	40
Fig.22.	Deflection Magnet Details.	44a
Fig.23.	Deflection Magnet as Installed.	44b

Fig. No.	List of Figures	Page No.
Fig.24.	Magnetic Saturation of Deflection Magnet.	47a
Fig.25.	Block Diagram of Magnet Current Regulator.	49a
Fig.26.	Circuit Diagram of Magnet Current Regulator.	50a
Fig.27.	Asymptotic Response of Magnet Current Regulator.	52a
Fig.28.	Deflection Magnet Controls.	52b
Fig.29.	Foil Wheel Determination of Proton Energy Spectrum.	55a
Fig.30.	Energy Spectrum of External Beam.	56a
Fig.31.	Double Focusing Sector-Shaped Magnet.	62a
Fig.32.	Energy Dispersion of Double Focusing Magnet.	64a

INTRODUCTION

A. General Introduction

The study of the nature of the atomic nucleus has long been hampered by a lack of knowledge of the forces which hold it together. A basic tool used in this study is the reaction of high energy particles with nuclei.

Much has been learned about the properties of these high energy reactions by studying the longer lived (> 0.1 sec) by-products of targets placed in the internal beam of synchro-cyclotrons. The internal beam, however, has a number of inherent limitations which prevent one from making the maximum use of the cyclotron. The targets placed in the internal beam must, in general, be removed from the vacuum tank after bombardment before they can be studied. This makes it impossible to study reaction products with very short lifetimes. Essentially instantaneous reactions such as scattering and fission are very difficult to study if the targets are inside the cyclotron tank. Because of the high vacuum, volatile targets cannot be bombarded unless encased in a vacuum-tight chamber. It is difficult to measure accurately the beam which hits an internal target, so a secondary standard monitor of known reaction cross section must be used.

An external proton beam does not have these drawbacks. Counting may go on continuously during the bombardment, or during the "quiet" period between beam pulses. This pulsed nature makes the beam ideal for the study of lifetimes between 50 μ sec and

2000 μ sec. Little work has yet been done in this field.

The external beam striking a target may be measured with fair accuracy, so the beam is very useful for the absolute determination of proton cross-sections.

Many proton scattering experiments have already been carried out with other external beams. Proton-proton scattering has been investigated in an attempt to determine the nature of the nucleon-nucleon forces. The results, particularly at high energies, do not conform to any simple model. The elastic and inelastic scattering of protons by heavier particles (deuterons and α-particles) and by nuclei have been observed for a few proton energies. The variation of the angular distribution of diffraction scattered protons with energy is a test of the validity of the Serber transparent nucleus model.[1]

Under certain conditions a scattered proton beam is highly polarized. Attempts have been made to explain the observations in terms of spin-orbit coupling.[2] Experimentally, this is of particular interest to those obtaining their external proton beams through coulomb scattering.

Many other more specialized fields are open for study with the external beam, particularly those employing nuclear plates, cloud chambers, and volatile targets such as liquids, gases or biological specimens. Unexpected effects may be found in this comparatively new field.

B. Discussion of Beam Extraction for Synchro-Cyclotrons

In the extraction of a proton beam from a high energy synchro-cyclotron, one finds the beam in a spiral so tightly wound that there is no room for the electrostatic deflection systems employed in fixed frequency cyclotrons. The internal beam consists of a 30 μ sec burst of pulses spiralling out in the cyclotron with a repetition rate of 200 / sec. At a radius of 36" (94 Mev protons) and a dee voltage of 6 Kv, the protons will spiral out about 0.001" per revolution. This small change in radius combined with the large momentum of the protons makes it impractical to use the customary electrostatic deflection system.

In order to be extracted, the beam must be deflected sufficiently to escape from the cyclotron field by itself (i.e. pass the n = 1 blowup radius) or must move into some region of reduced field which "peels" it off. Many types of extraction systems have been suggested, but only three or four have been satisfactorily operated.

Extraction Systems

(1) Electrostatic Deflector

One type of electrostatic deflector consists of four bars positioned in a square array above and below the beam. A high voltage pulse is applied to the system when the beam reaches its centre, deflecting the beam into a magnetically shielded channel. A high yield is theoretically possible with this system, but a very short, very intense burst of particles is obtained. This method has been used with only moderate success in the Berkeley 184 in. synchro-cyclotron.

(2) A Coulomb Scattering Deflector

The proton beam undergoes coulomb scattering from a heavy target. A portion of the beam which is scattered horizontally outward at a small angle is peeled out by a magnetically shielded channel. This system will be described later in greater detail. It has the advantages of simplicity and comparatively long pulse length. The efficiency of this system, however, cannot be better than 10^{-4}.

(3) Regenerative Magnetic Extractor

The regenerative magnetic extractor was first proposed by Tuck and Teng[3,4] and has been successively operated for the first time at Liverpool.[5] This regenerative system consists of a "peeling" region in which the magnetic field falls off rapidly with radius, followed in 60° azimuth by a "regenerating" region in which an increase in field takes place. These magnetic discontinuities produce a radial oscillation which grows exponentially in amplitude, so that the beam may jump out into the magnetic channel between the two discontinuities.

(4) "Spill Out" Extraction System

In some synchro-cyclotrons it is possible to accelerate the beam to the n = 1 "spill out" radius without losing much of its intensity due to vertical blow up at the n = 0.2 radius. At this point it escapes more or less isotropically from the magnetic field, so a window in the wall of the chamber will pick up a portion of this beam.

C. Preliminary Beam Extraction Work at McGill

(1) Beam Extraction

In 1951 an attempt was made by Dr. D. Hone to extract the cyclotron beam with a pulsed electrostatic deflector.[6] He applied a 100 Kv pulse of 0.045 μ sec duration to a four bar electrode system covering 90° in azimuth. With this he succeeded in deflecting a large fraction of the beam 0.5" out from the 36" radius orbit. The critical nature of this system and short pulse length made it appear advisable to try another type of extraction.

A new system was desired whose installation would result in a minimum of shut-down time for the cyclotron. The most feasible one was the coulomb scattering deflector and magnetic channel which is comparatively simple and could be installed quickly. In this system, the proton beam impinges upon a high atomic number target which elastically scatters it. Those protons which are scattered horizontally outward at an angle of 4 to 5 degrees may pass between the bars of a soft iron channel, which reduces the magnetic field. This channel peels the beam completely out of the cyclotron.

The design and testing of a preliminary extraction system was carried out here by Dr. J. S. Kirkaldy.[7] The beam was scattered by a 4 mil. uranium target positioned at a radius of 36" and 63.6° in azimuth before a magnetic channel. This channel, whose entrance was at a radius of 38.2", accepted protons scattered outward through an angle of 4.5°. At the exit of the channel a beam of approximately

4×10^{-13} amps was measured - less than 1 per cent of the theoretical yield. It was thought that either the $\frac{3}{4}$" radial oscillation amplitude assumed for the channel position determinations was too small, or the beam was undergoing a premature blowup before hitting the target.[8] Later measurements indicated that the mean radial oscillation amplitude is close to 1". Careful magnetic field measurements also showed that a centre shift in the equilibrium orbit may have prematurely brought part of the beam into a high field gradient region (n = 0.2) where a vertical blowup of the beam could occur.

(2) Shielding and Focusing

The neutron background in the cyclotron room is very high. Several feet from the magnet coils behind 13" of concrete the background was measured to be 5×10^5 neutrons/cm^2/min with an energy above 20 Mev.[9] These would produce a background of about 10 counts / sec in the proton telescope built here for use with the external beam. This background is of the same order as the expected counting rate for many types of scattering experiments. It was very desirable, therefore, to shield the equipment better.

EXPERIMENTAL WORK

A. General Programme

The McGill synchro-cyclotron is capable of producing a pulsed beam of protons with a maximum energy of 95 Mev (36" radius). It is operated with a maximum oscillator voltage of 7 Kv applied to a single radio frequency dee. A dummy dee opposite the radio frequency dee is at a floating potential. The frequency is modulated by a rotating condenser with a repetition rate of 200 cycles per second. An average internal beam current of about 0.8 μa is commonly obtained.

The failure of the preliminary extraction attempt was attributed to a premature blowup of the beam because of high field gradients in the cyclotron and to errors in the channel positioning caused by an incorrect knowledge of the proton energy. It was hoped to eliminate these factors by a careful shimming of the magnetic field of the cyclotron, and by subsequent measurements of the beam centre shifts and radial oscillation amplitude.

The preliminary work also indicated that much better shielding of the experimental apparatus was necessary if one were to keep the background at a reasonable level. The 11 foot shielding wall between the cyclotron room and the entrance corridor is an excellent shield, but in normal operation the extracted beam would be in the wrong direction to utilize it. If, however, the magnetic field of the cyclotron were reversed, a counterclockwise moving beam would be obtained. A portion of this beam could be conveniently

extracted from the cyclotron vacuum chamber at the ion source box (see Fig. 1). These protons, if bent through 45°, would pass through the 11 foot wall into the corridor. To deflect the beam, a large electromagnet was proposed. This magnet could also focus the divergent beam on to a small target in the corridor. This way out of difficulties was suggested by the Director.

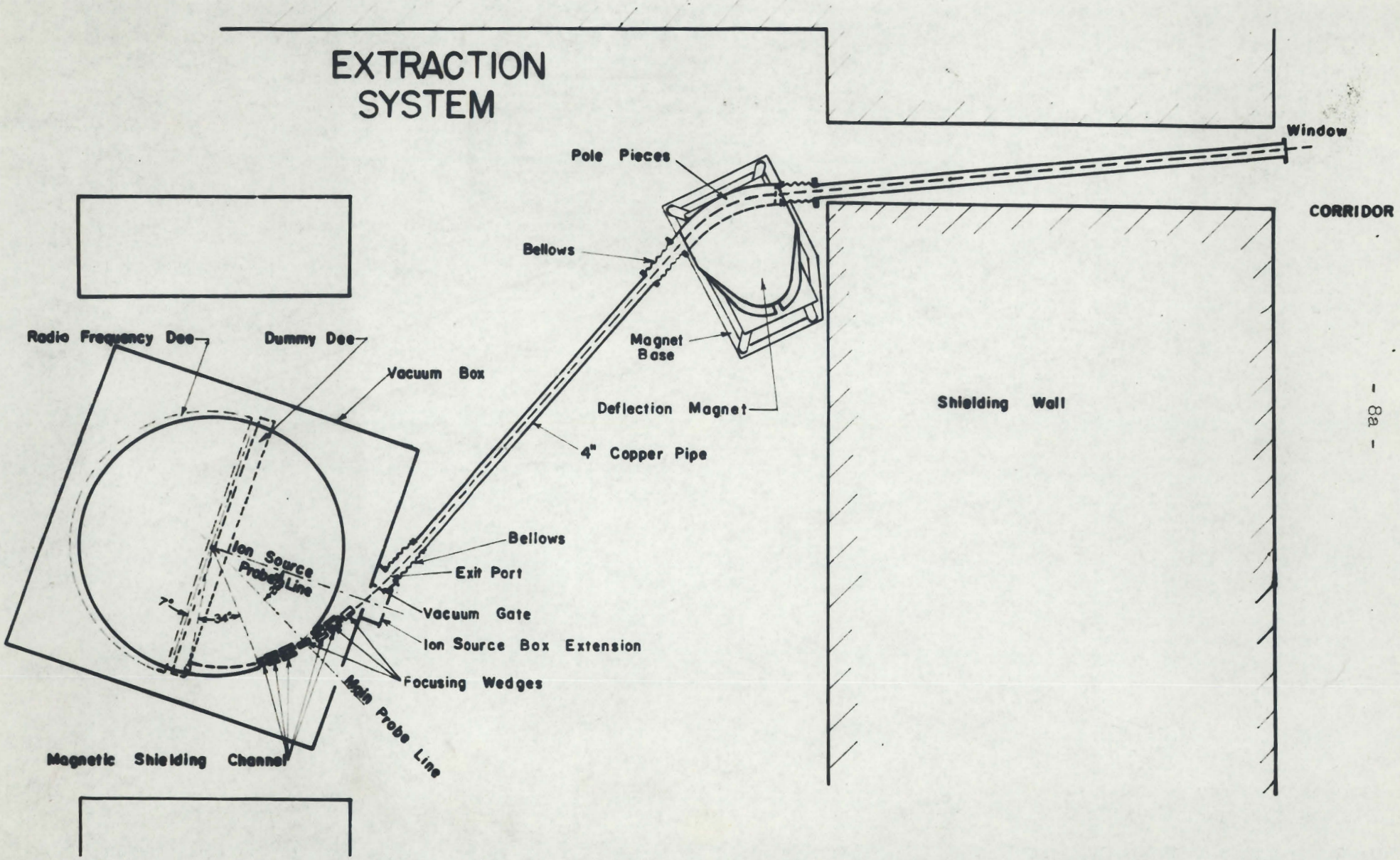
EXTRACTION SYSTEM
Window
Pole Pieces
CORRIDOR
Bellows
Magnet Base
Radio Frequency Dee
Dummy Dee
Vacuum Box
Deflection Magnet
Shielding Wall
4" Copper Pipe
Bellows
Ion Source Probe Line
Exit Port
7°
34"
Vacuum Gate
Ion Source Box Extension
Focusing Wedges
Main Probe Line
Magnetic Shielding Channel

Fig.1.

B. Installation of the Extraction System

(1) General Shimming of the Magnetic Field

Alignment of the magnetic channel is critically dependent upon the energy and spectrum of the beam hitting the target. The protons strike the scattering target when close to the maximum outward swing of their radial oscillation, hence the energy of the scattered protons is less than the nominal energy at this radius by the energy equivalent of the radial oscillation amplitudes. In addition, the proton energy will be changed by a shift of orbit centres away from the geometric centre of the cyclotron. This shift is given to the first order by $\delta = A_1/\frac{dB}{dr}$ where A_1 is the amplitude of the first harmonic of the field inhomogenuities.

In an attempt to reduce the radial oscillation amplitude of the internal beam, and to prevent its premature blowup, a general shimming of the cyclotron magnet was undertaken. The field was measured with an integrating fluxmeter[10] whose most sensitive range is 100 gauss full-scale. The search coil is mounted on a horizontal motor driven arm, pivoted at the centre of the cyclotron, and the flux change is continuously recorded on an Esterline Angus recorder. With this instrument deficits of some 30 gauss were found along the south side of the magnet, as well as periodic deficits at the corners of the vacuum chamber. This was enough to shift the centre of the proton orbit up to 3/4" away from the low field region. These

deficits were removed by contour shims inserted under the $\frac{1}{2}$" pole faces. The azimuthal fluctuations from the mean at any given radius were thus reduced to less than ± 10 gauss, and the beam centre shift to less than 0.1".

The beam had previously blown up very rapidly as it approached a radius of 36" except for a "hard" central core which appeared to undergo no radial oscillations. A series of glass plates bombarded at different radii shows no indication now of this hard core (Fig. 2), but approximately 2/3 of the beam is still lost before it reaches the 36" radius. The internal energy spread of the beam at 36" was redetermined using a teflon target in the 180° internal scattered beam. This technique is described in detail in a McGill Radiation Laboratory report.[8] The measured mean radial oscillation amplitude is 1.1" and the full energy width at 1/2 maximum is 8.1 Mev. The spectrum is compared with the one obtained before re-shimming in Fig. 3 . The observed tails on the distribution curve are probably due to scattered protons and to the 1.5 Mev resolution of the system. The target was scanned in $\frac{1}{4}$" strips on a single channel NaI spectrometer set on the 511 Kev peak of the annihilation radiation from the 20.5 min. C^{11} β^+ activity.

(2) Theoretical Location of the Scatterer and Magnetic Channel

(a) General Considerations

The principal variable parameters in the extraction problem are the target radius, the angle of scattering, the target thickness, and the azimuthal angle between the scatterer and the magnetic

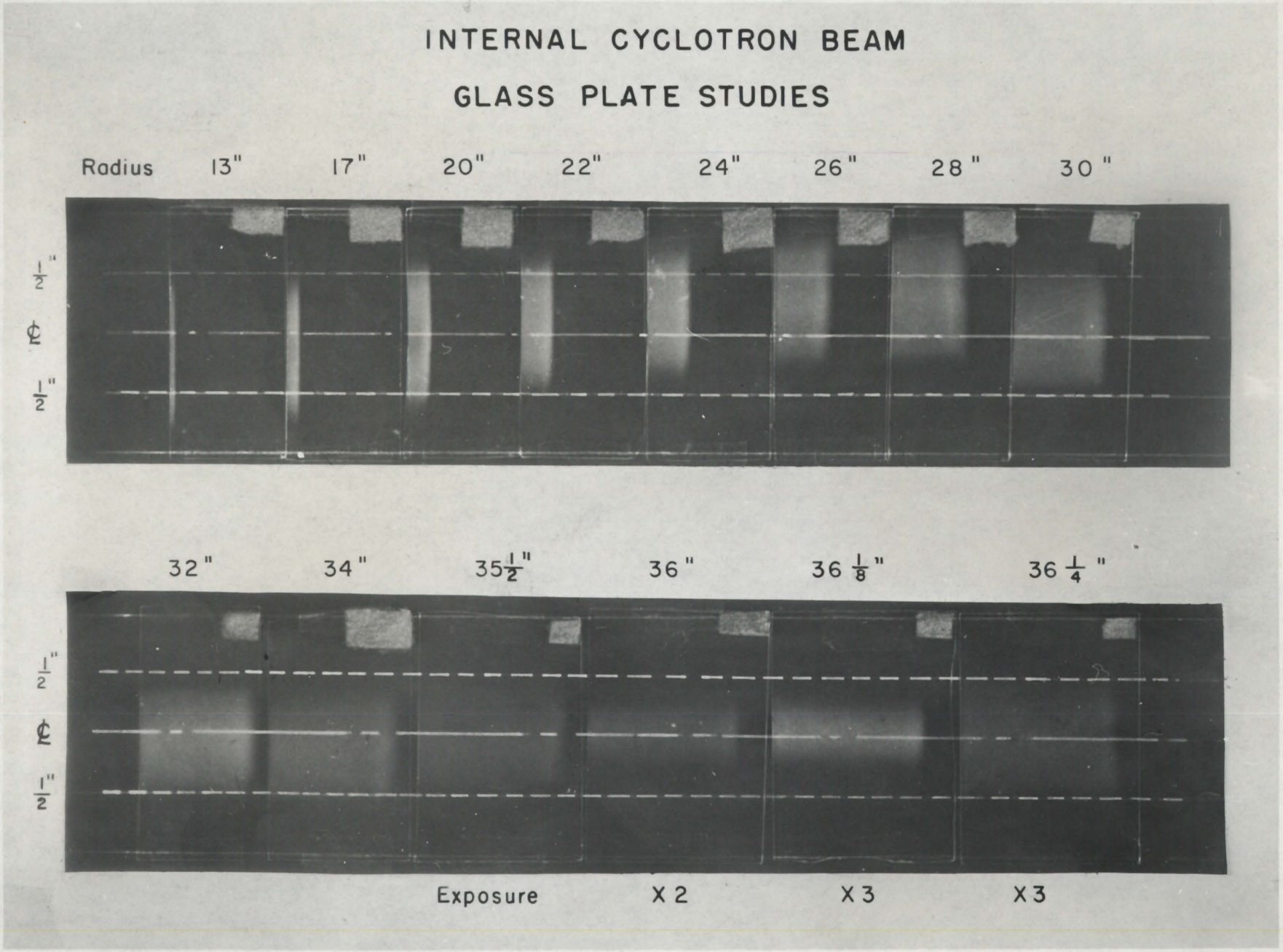
INTERNAL CYCLOTRON BEAM
GLASS PLATE STUDIES
Radius 13" 17" 20" 22" 24" 26" 28" 30"
½"
℄
½"
32" 34" 35½" 36" 36 ⅛" 36 ¼"
½"
℄
½"
Exposure X 2 X 3 X 3

Fig.2.

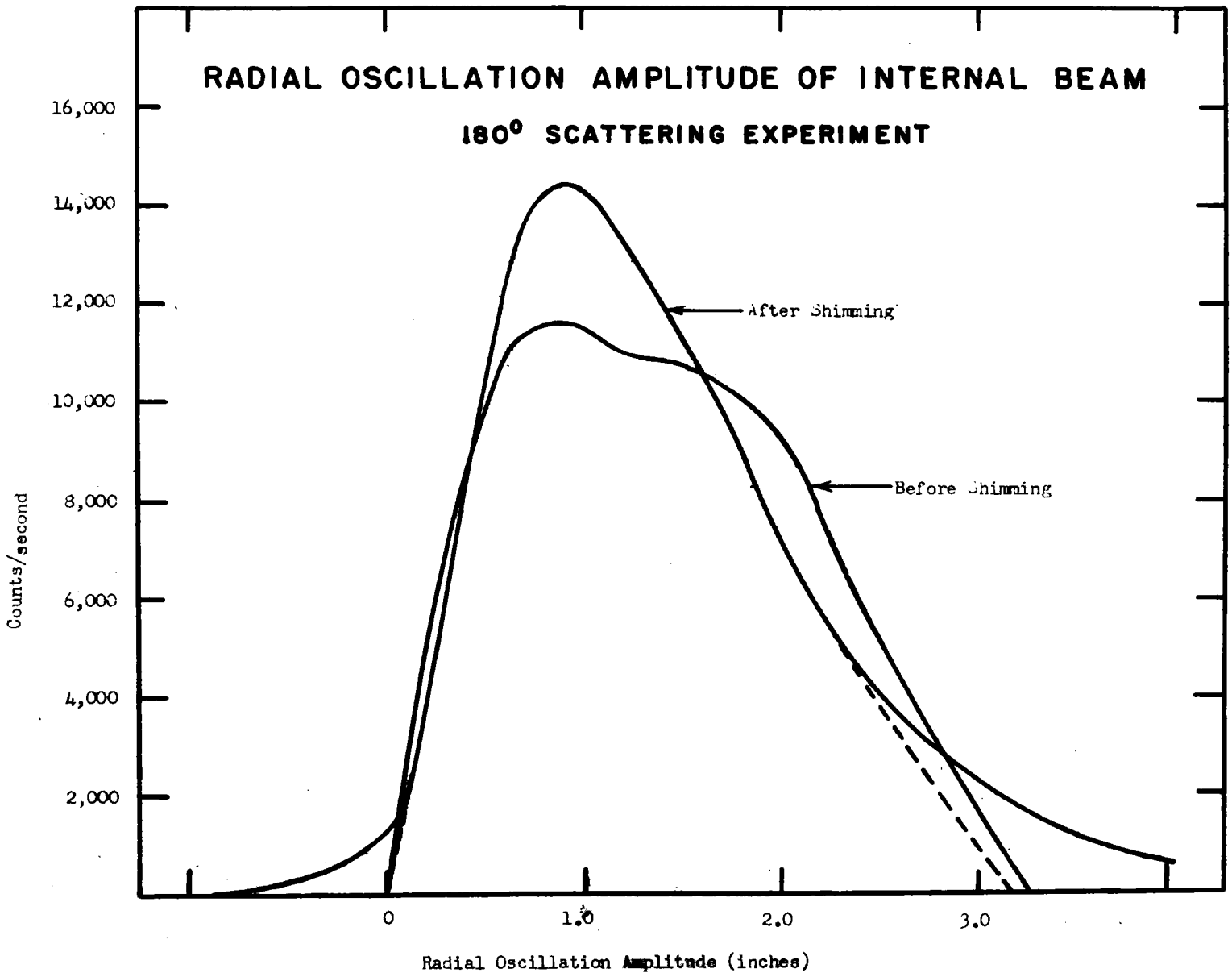
RADIAL OSCILLATION AMPLITUDE OF INTERNAL BEAM
180° SCATTERING EXPERIMENT
16,000
14,000
12,000
10,000
8,000
6,000
4,000
2,000
Counts/second
After Shimming
Before Shimming
0
1.0
2.0
3.0
Radial Oscillation Amplitude (inches)

Fig.3.

channel. There are also a number of fixed parameters which must be considered.

(i) The minimum radius of the entrance to the magnetic channel is about $1\frac{3}{4}$" greater than the scattering radius. This is due to the physical size of the channel and to the necessity for shimming out deficits in the magnetic field at 36" caused by the channel.

(ii) The average radial oscillation amplitude of the protons is approximately 1".

(iii) Single coulomb scattering in the target is assumed.

(iv) The small change in magnetic field with radius was considered negligible.

(v) The total beam extracted rather than the beam density at the exit port is the initially important factor, since it is assumed that the beam may subsequently be focussed into a small area.

The accompanying diagram illustrates the scattering extractor from a geometrical point of view. The proton beam hits the target at radius r, and is scattered outward through the angle ϕ. The radius of curvature of the beam is now $\rho = r - A_r - \delta$ where A_r is the mean radial oscillation amplitude, and δ the decrease in radius caused by the energy loss in the target.

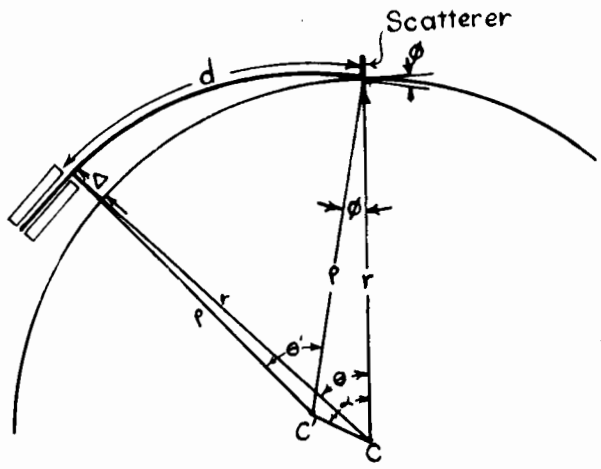

Fig.4.

From a geometrical analysis, it can be shown that the difference Δ between the beam radius and the scattering radius at azimuth angle θ is given by

$$\Delta \cong \rho - r + \frac{\rho \phi}{\sin\alpha} \cos(\alpha - \theta)$$

for small ϕ and where $\alpha = \mathrm{Tan}^{-1} \frac{\rho\phi}{r-\rho}$.

Solving for the angle of azimuth θ one obtains

$$\theta = \alpha - \cos^{-1}\left\{\frac{\sin\alpha}{\rho\phi}(\Delta + r - \rho)\right\}.$$

The efficiency of the extraction system is defined as

$$\eta = \frac{\text{number of particles passing through the channel}}{\text{number of particles hitting the target.}}$$

This efficiency is determined by the differential scattering cross-section at the angle ϕ and the solid angle subtended by the channel entrance. Hence

$$\eta = \left\{\frac{d\sigma}{d\Omega} \cdot N \cdot t\right\}\left\{\frac{A}{d^2}\right\}$$

where N is the nuclear density in nuclei/gm,

t is the target thickness in gms/cm^2,

A is the effective entrance aperture of the channel,

d is the path length from the scatter to the channel,

and $\frac{d\sigma}{d\Omega}$ is the differential scattering cross-section per unit solid angle.

The differential cross-section for single coulomb scattering of a particle carrying charge Z' by a nucleus of atomic number Z is

$$\frac{d\sigma}{d\Omega} = \left(\frac{Z\,Z'\,e^2}{2\,m v_o^2}\right)^2 \sin^{-4}\frac{\phi}{2}$$

For small angle scattering of protons this becomes:

$$\frac{d\sigma}{d\Omega} = 4\left(\frac{Ze^2}{mv^2}\right)^2 \frac{1}{\phi^4}$$

Expanding this equation in terms of the relativistic particle energy one obtains

$$\frac{d\sigma}{d\Omega} = 4\left(\frac{Ze^2}{\frac{E^2 + 2Em_oC^2}{E + m_oC^2}}\right)^2 \frac{1}{\phi^4} \text{ cm}^2 \text{ / nucleus / unit solid angle}$$

The scattering cross-section for 90 Mev protons incident upon a uranium target of thickness t gms/cm^2 is then

$$\frac{d\sigma_v}{d\Omega} = 6.05 \times 10^{-5} \frac{t}{\phi^4}$$

The angle of azimuth θ and the extraction efficiency were calculated for several scattering angles and target thicknesses. Fig. 6 shows the variation of the efficiency with the azimuth angle for a wide range of target thicknesses. Fig. 6 illustrates the variations of the extraction efficiency with target thickness for several scattering angles. From these curves, the following general conclusions may be drawn:

(i) If the entrance of the channel is placed at a fixed radius, there is little change in the extraction efficiency for a wide variation of the azimuth angle between the scatterer and the mouth of the channel.

(ii) The efficiency increases with increasing target thickness. The maximum efficiency attainable is limited by the energy

Fig.5.

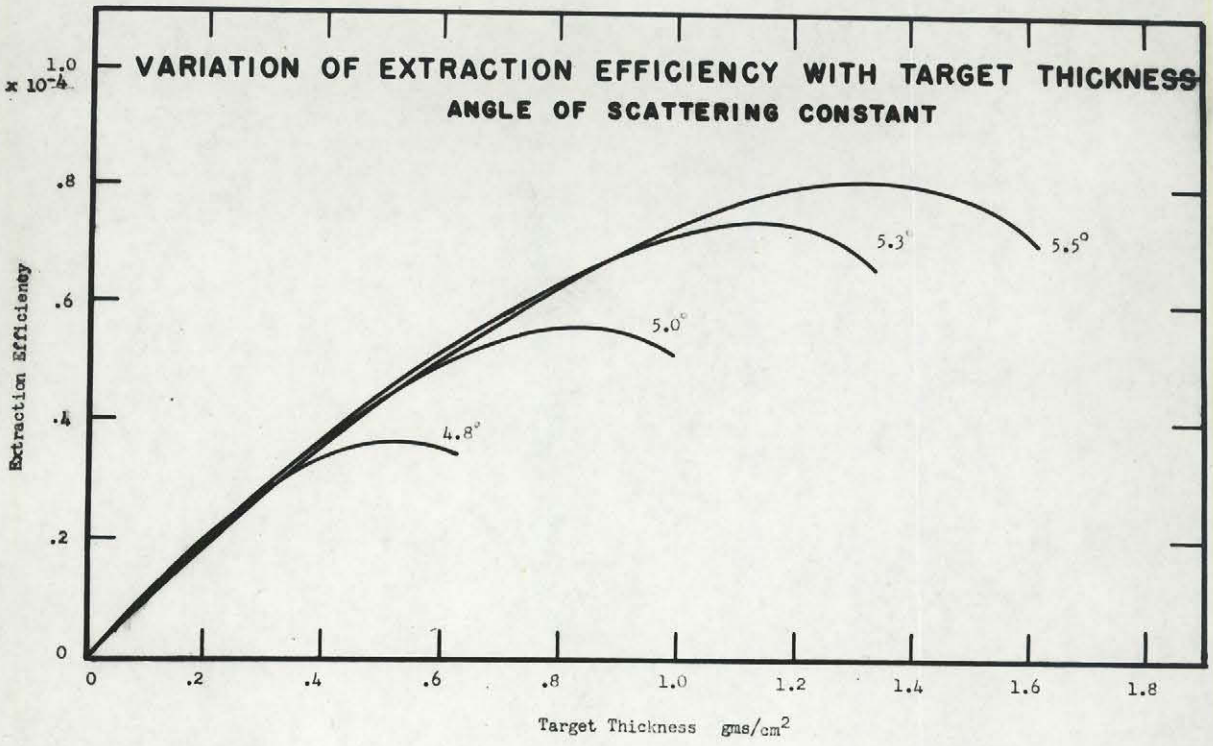
VARIATION OF EXTRACTION EFFICIENCY WITH TARGET THICKNESS
ANGLE OF SCATTERING CONSTANT
1.0 x 10-4
.8
.6
.4
.2
0
Extraction Efficiency
5.3°
5.5°
5.0°
4.8°
0
.2
.4
.6
.8
1.0
1.2
1.4
1.6
1.8
Target Thickness gms/cm2

Fig.6.

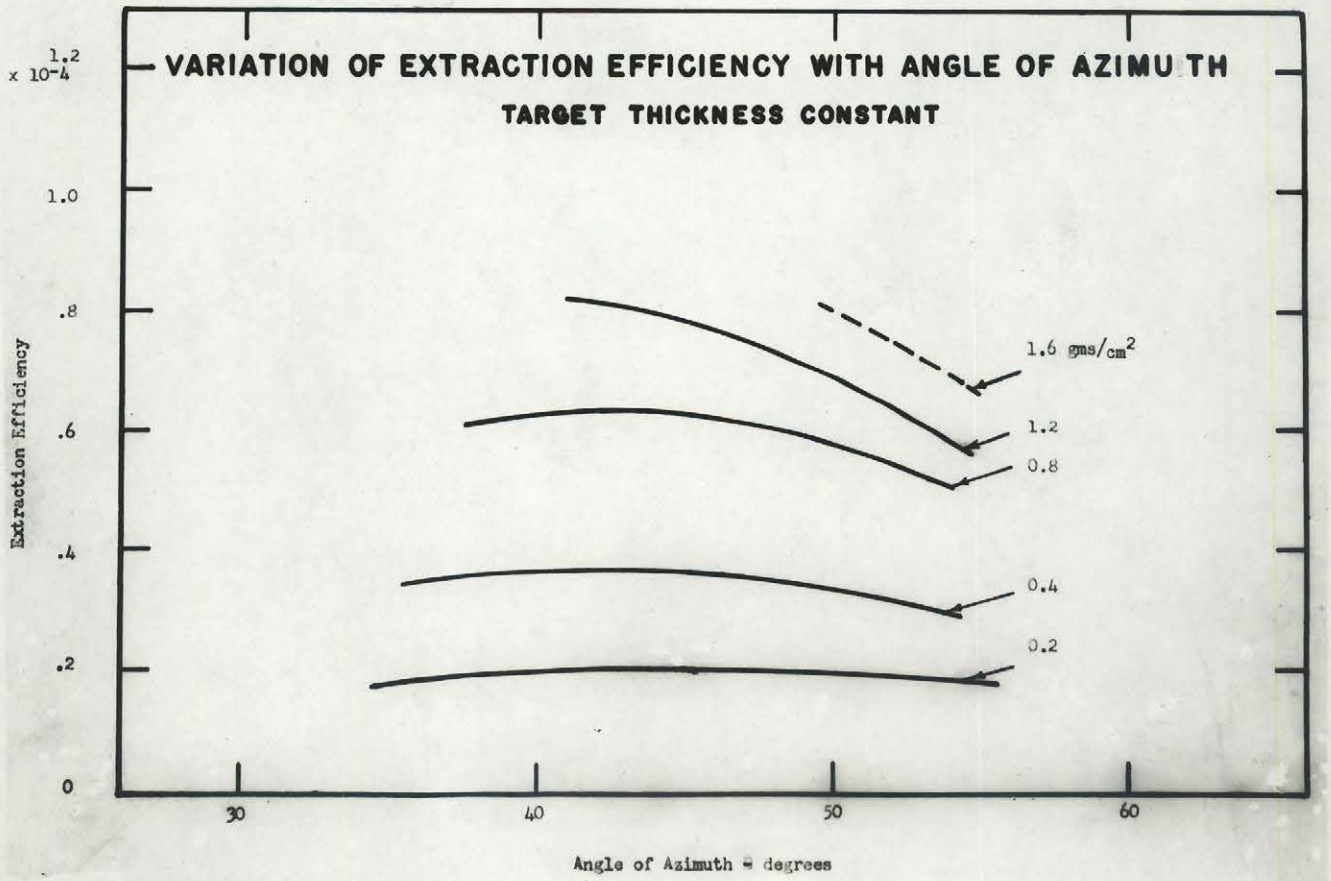
VARIATION OF EXTRACTION EFFICIENCY WITH ANGLE OF AZIMUTH
TARGET THICKNESS CONSTANT
1.2 x 10-4
1.0
.8
.6
.4
.2
0
Extraction Efficiency
1.6 gms/cm2
1.2
0.8
0.4
0.2
30
40
50
60
Angle of Azimuth = degrees

loss in the target.

(iii) The "optimum" condition for this hypothetical case (considering a reasonable energy loss in the target) appears to be scattering through an angle of 5.5° by a 1.3 gm/cm^2. uranium target placed at an angle of about 45° from the channel mouth. The theoretical efficiency for these conditions would be 0.82×10^{-4}.

For simplicity, these calculations have neglected the significant decrease in the magnetic field with radius. Its chief effect would be to allow protons normally scattered through smaller angles to enter the channel. In addition, multiple coulomb scattering tends to flatten out the peak in the forward direction, which would make it profitable to move the magnetic channel closer to the scatterer. It was estimated (and subsequently proven by a ray trace) that the scattering angle under these optimum conditions would be closer to 5°.

(b) Ray Tracing Method

In order to learn the "peeling" effect of the channel and thus find where the beam would hit the cyclotron wall, a ray trace of the protons through the changing magnetic field was carried out.

Referring to Fig. 7 , the motion of a proton in a magnetic field is given by

$$\text{Tan } \phi = \frac{1}{r} \cdot \frac{dr}{d\theta}$$

and

$$\frac{r}{\rho} = \text{Cos } \phi \left(1 + \frac{d\phi}{d\theta}\right).$$

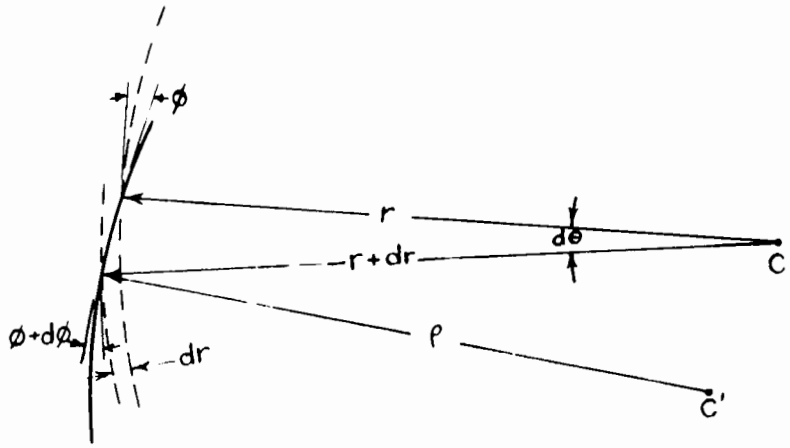

Fig.7.

These reduce to forms easily integrated algebraically.

$$d\emptyset = d\theta \left(1 - \frac{r}{\rho} \operatorname{Sec} \emptyset\right)$$

and $dr = r\, d\theta \operatorname{Tan} \emptyset$

The following initial conditions were assumed:

(a) Scattering at 36" (r_o = 36")

(b) $\emptyset_o = 5^\circ$

(c) ρ_o = 34.25". This corresponds to a mean radial oscillation of 7/8" and a target energy loss of 4.5 Mev by a 1.2 gm/cm^2 uranium target.

(d) $d\theta = 5^\circ$. The magnetic channel begins at $\theta = 40^\circ$

(e) The shielding ratio of the channel was estimated to be 2.5 in accordance with previous measurements.[7] This figure now appears to be somewhat low. The channel consists of four sections covering an angle of 25°.

(f) The variation of the magnetic field with radius was taken from a recent field plot.

The path followed by the scattered beam according to the ray tracing plot is shown in Fig. 8 . The channel position is a convenient one used in the preliminary extraction attempt and the scatterer is mounted inside the radio frequency dee. This calculation indicates that the beam would emerge from the vacuum chamber between the main probe and the ion source probe. A simple shift of the system around a few degrees to bring the beam out at the ion source port is not possible because of the interference of the magnetic channel with other apparatus (i.e. scattering probe and main target probe). This shift was finally brought about, however, by splitting the channel into two parts, which straddle the main probe, one of three sections and the other a single section.

(3) Installation of the Magnetic Channel

(a) Positioning of the Channel

The magnetic channel, as first installed, consisted of one $2\frac{1}{2}$" long section followed by three 5" sections. The separation and height of the channel sections were successively increased to allow for the divergence of the beam. The sections were mounted on adjustable platforms for convenience in alignment.

Since the channel alignment is critically dependent upon the estimated shielding effect of the channel, the stretched current-carrying wire technique was employed to determine the true path of

RAY TRACING PLOT FOR BEAM EXTRACTION

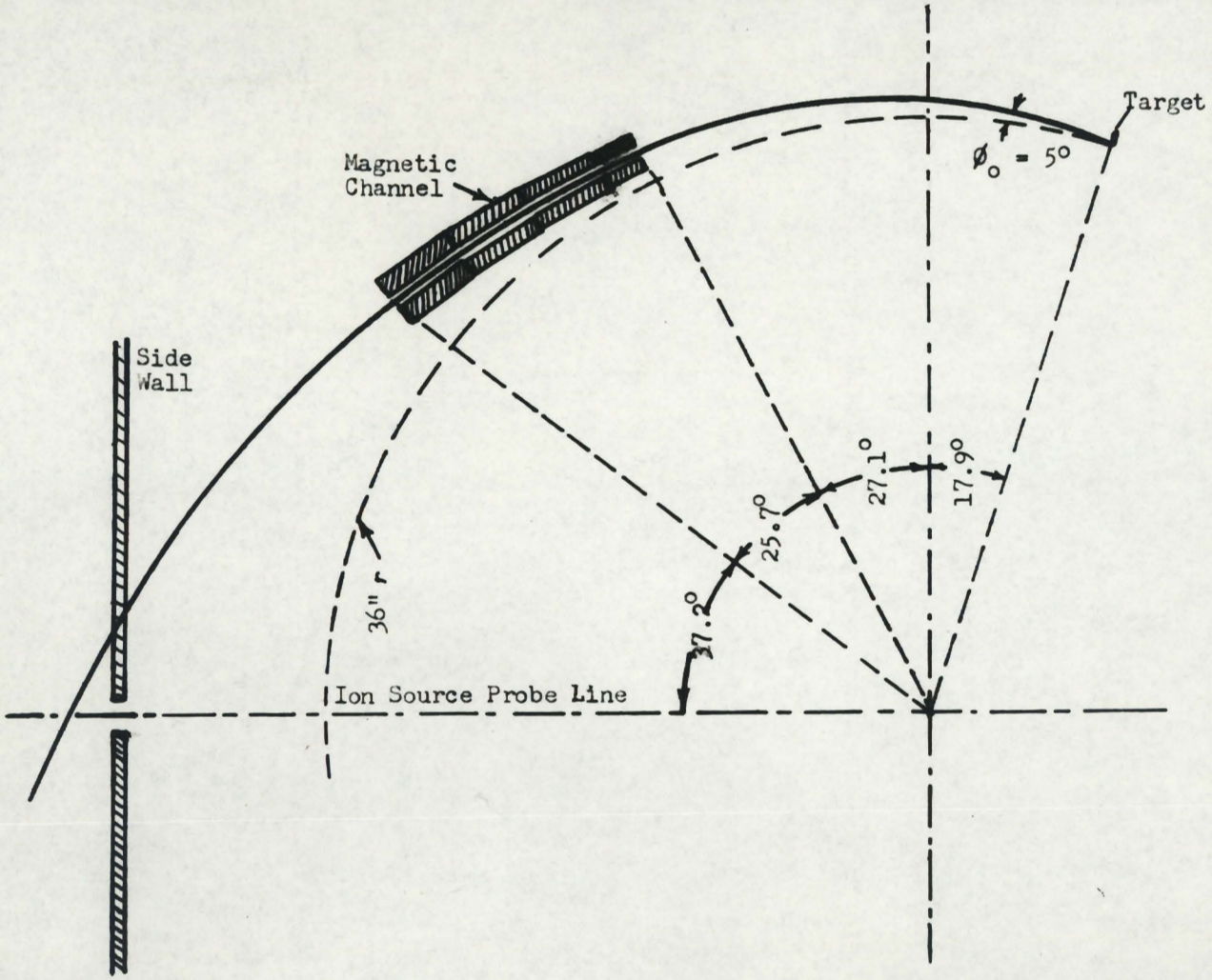

Fig.8.

the protons.

The path of a charged particle moving in a magnetic field is duplicated by a flexible current-carrying wire, subject to a certain current-tension relationship. This relationship is

$$B\rho = \frac{p}{q} = \frac{T}{I}$$

where B is the flux density (webers/meter^2)

ρ is the radius of curvature (meters)

p is the momentum (Kg meters/sec)

q is the electric charge on the particle (coulombs)

T is the tension on the wire (Newtons)

and I is the current in amps.

This equation becomes

$$0.1401\ I = W$$

for protons with an energy of 88 Mev and the tension T being applied by a weight W Kg hanging over a frictionless pulley.

One end of a length of No. 32 wire was fixed at the scatterer position; the other end passed through the ion source port and over an aluminum pulley mounted outside the magnetic field. The tension produced by a 200 gm weight with an associated current of 1.428 amps was found to give satisfactory results.

Using this technique the channel was carefully aligned and fixed in its new position. The entrance to the first short section of channel was set at $37\frac{3}{4}$" and this permitted the proper shimming of the field at $36\frac{1}{4}$" to recover the normal value. The channel does not interfere with necessary mountings on the main

probe which clears the channel by 1.2" and 2" at inner and outer sides of the channel respectively. The general physical layout may be seen in two photographs (Fig. 9 (a), (b)). The scattered targets are conveniently mounted in the dummy dee at an azimuthal angle of 34° from the channel.

(b) Reshimming the Magnetic Field

The magnetic channel draws flux from the surrounding areas, thus producing deficits in the field which must be removed if the proton beam is not to be disturbed. Fig. 10 shows the field deficit contours at various radii before the reshimming. These measurements were made with the integrating magnetic field fluxmeter which was altered to give a slow scan. Marker pips every 15° in azimuth locate the position of the field measuring coil.

A combination of vertical iron plate shims and horizontal contour shims were utilized to remove this deficit. The vertical plates are $1\frac{1}{16}$" wide, $\frac{1}{16}$" thick and vary in length from 2" to $\frac{1}{2}$". They are mounted in two parallel rows at radii of 36" and $36\frac{3}{4}$".

Since the magnetic field contours could be determined very quickly, the "cut and try" method was used to position the shims. The shimming was so critical that it was possible to see a significant effect for a $\frac{1}{4}$" change in the length of one shim. By careful adjustment of the shims, the magnetic field at the 36" radius was smoothed out to within $\pm$ 30 gauss from the mean. A large deficit of 130 gauss still exists over a small area at the

INITIAL BEAM EXTRACTION INSTALLATION

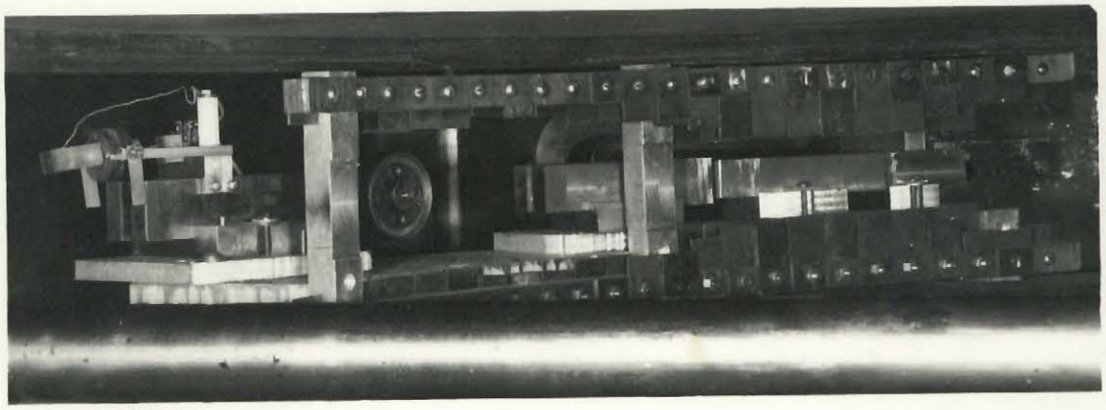

(a) The Initial Magnetic Shielding Channel Installation.

Note the four channel sections (centre, left to right) and the vertical plate shims.

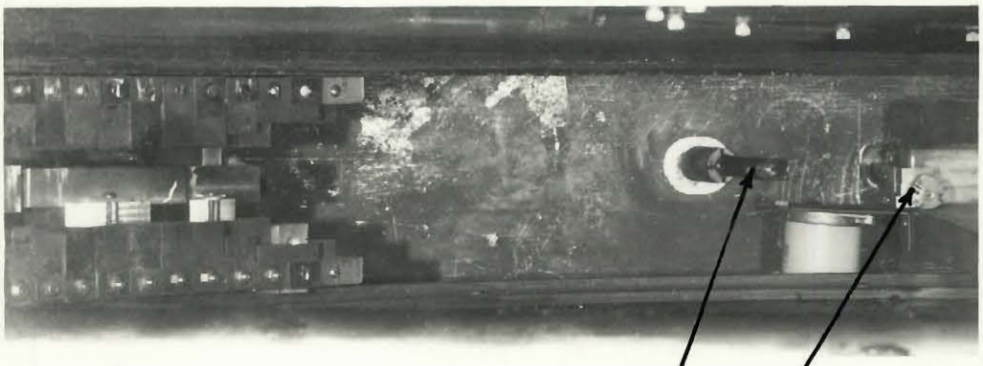

(b) Coulomb Scatterer and Magnetic Channel.

The relative positions of the scattering target and magnetic shielding channel are clearly seen. The rod projecting through the side wall of the cyclotron is used to adjust the target radius, and to alter the target thickness.

Fig.9.

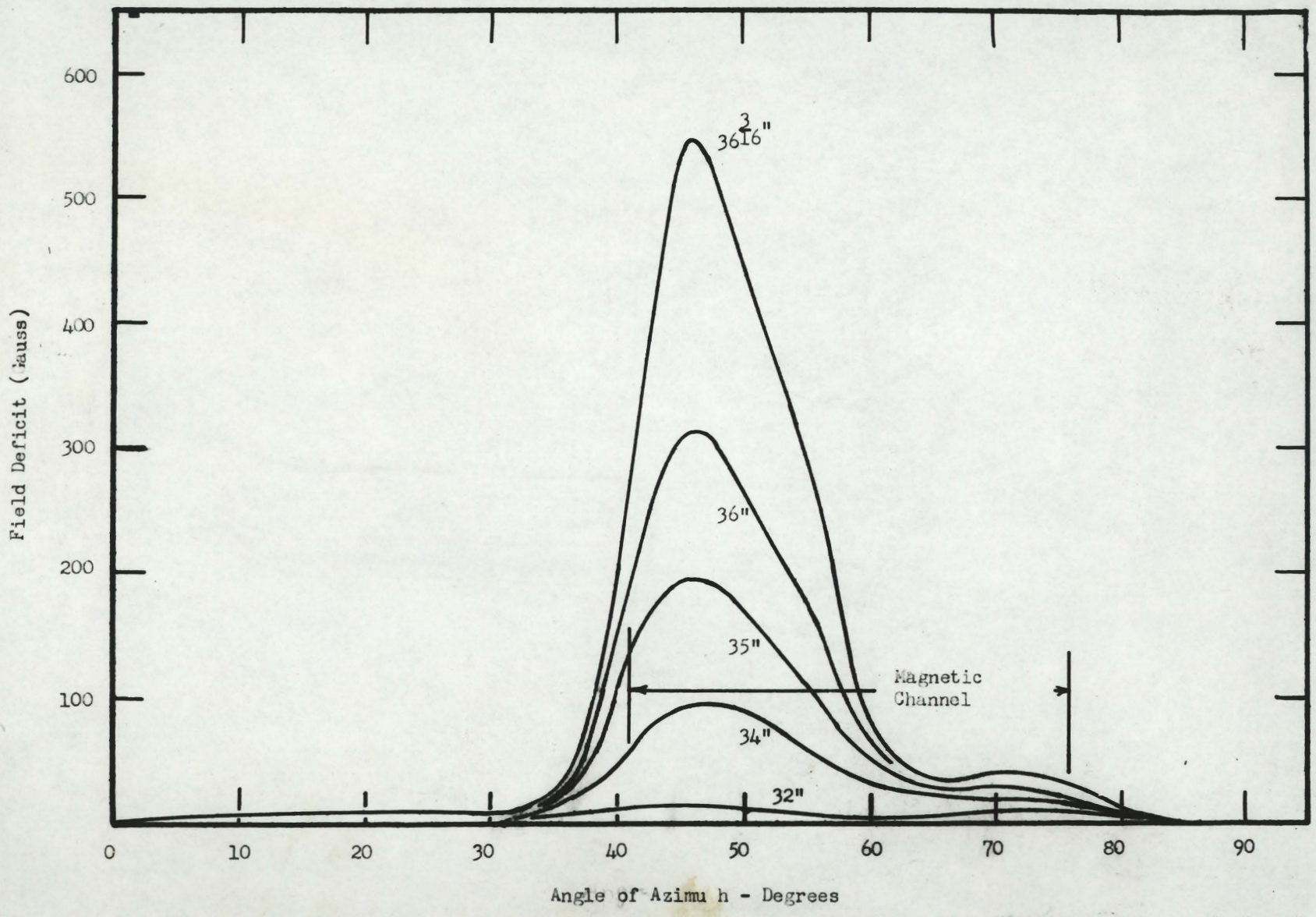
FIELD DEFICIT BEFORE SHIMMING
Field Deficit (Gauss)
600
500
400
300
200
100
0
10
20
30
40
50
60
70
80
90
Angle of Azimu h - Degrees
3/16"
36"
35"
34"
32"
Magnetic Channel

Fig.10.

$36\frac{1}{4}$" radius, but since most of the beam had already blown up before this point, no further shimming was attempted.

When the large field deficits had been removed, a general deficit of up to 50 gauss still remained over a sector 25° wide extending from the 32" to the 36" radius. A shim built up from five different-sized contours of 0.01" silicon steel was inserted under the $\frac{1}{2}$" pole piece to remove this deficit. A reproduction of the recorder chart (Fig. 11) illustrates the final field contours. A full-scale reading on the chart corresponds to 500 gauss.

(c) The Scattering Targets

Three scattering targets of different thicknesses are mounted on a vertical disc in such a way that a rotation of the disc moves any target in turn up into the median plane between the pole-pieces. A rotation of the disc also moves it in and out on a screw thread (see Fig. 12 for details). In this way any one of the three targets may be utilized at a radius from $35\frac{5}{8}$" to $36\frac{5}{8}$" in steps of $\frac{1}{32}$". The targets first used were of uranium, 0.41, 0.62, and 1.04 gm/cm^2 respectively. These were later exchanged for two uranium targets of 0.62 and 1.46 gm/cm^2 and a 2.5 gm/cm^2 tungsten target. This tungsten target was used because no uranium of the proper thickness was immediately available. The scattering from the tungsten target is 0.87 that from an equivalent uranium target, and the energy loss is 1.07 times greater.

FIELD CONTOURS OF CYCLOTRON MAGNET

AFTER SHIMMING OUT EFFECTS OF THE MAGNETIC CHANNEL

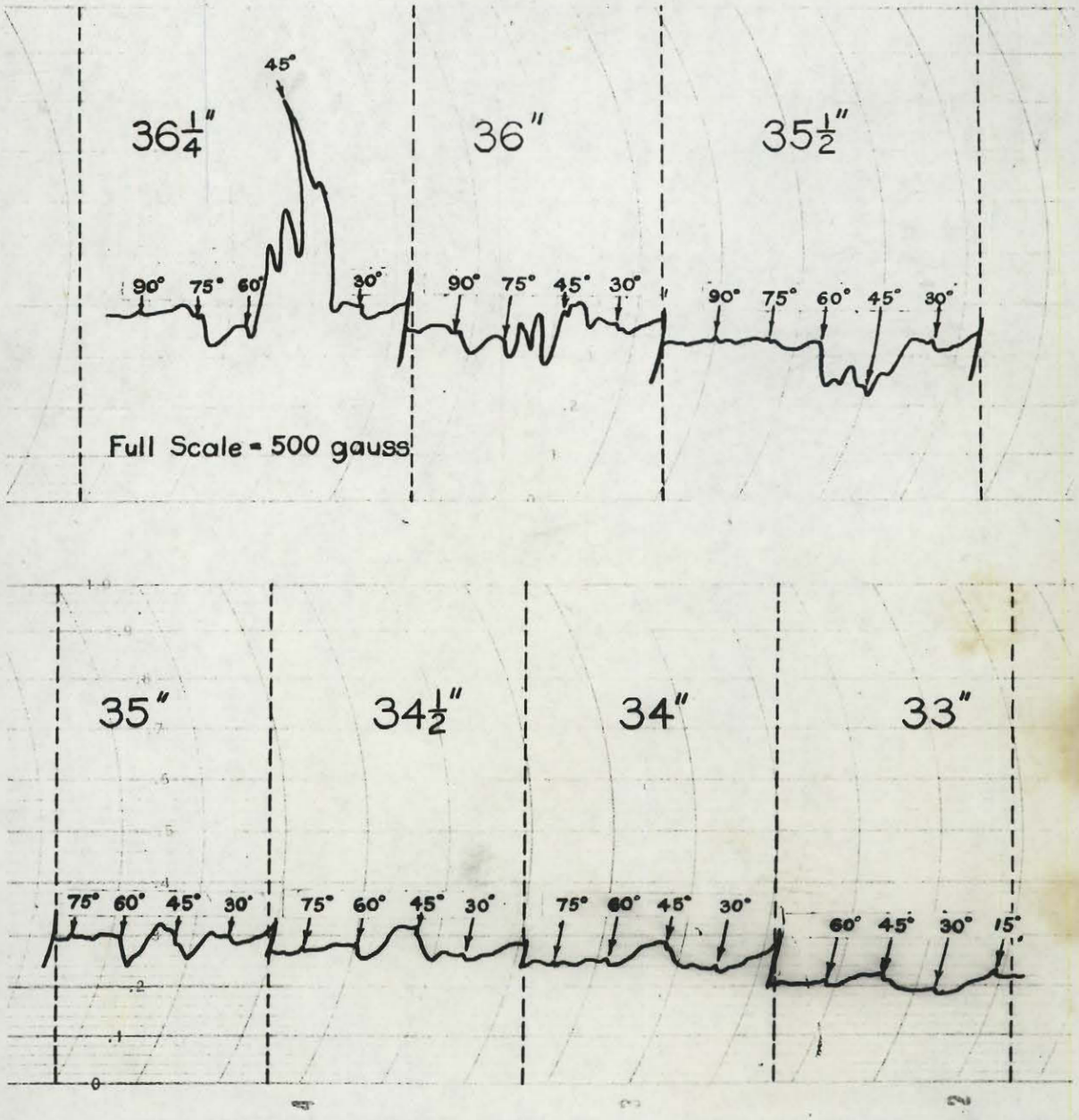

Fig.11.

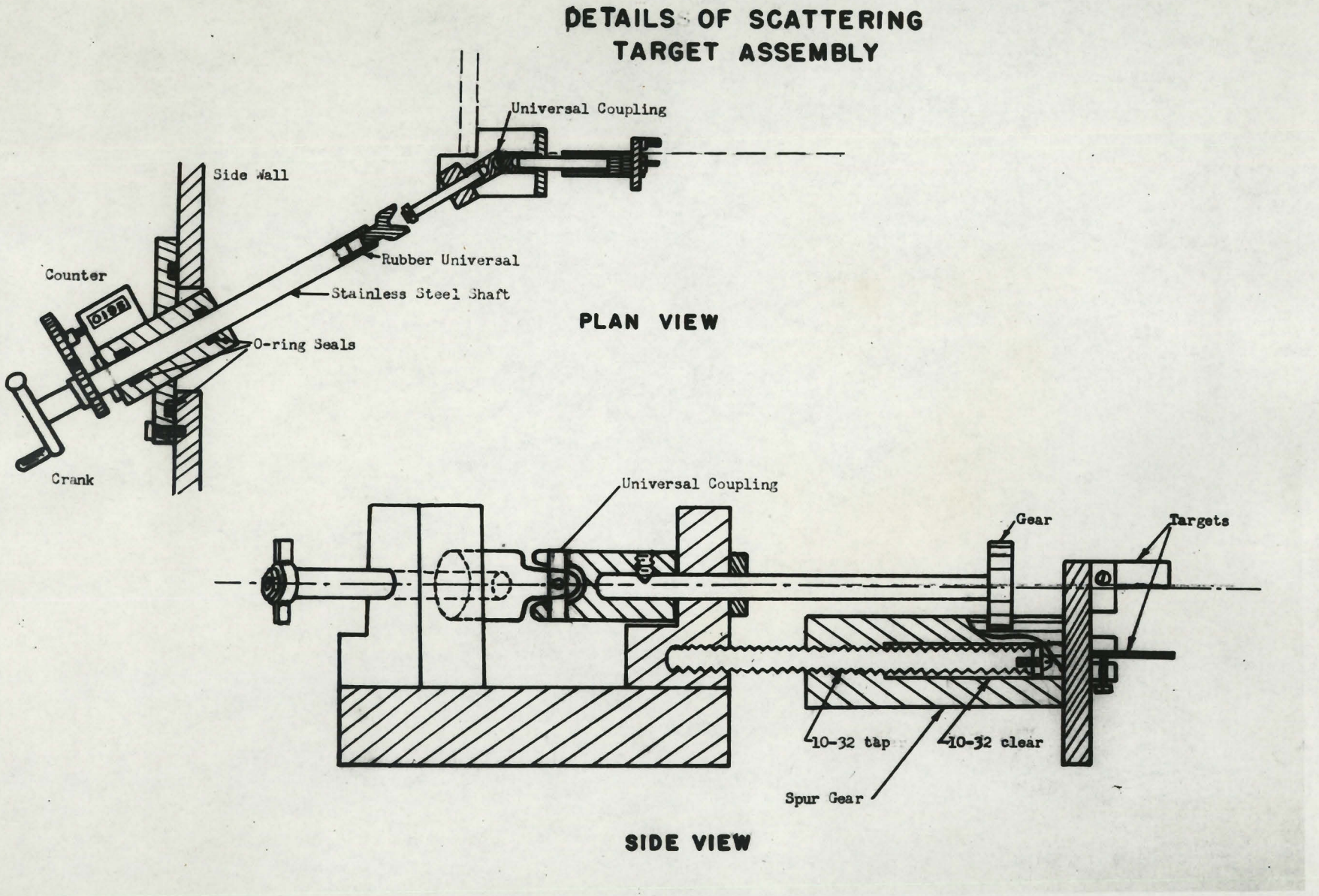
DETAILS OF SCATTERING
TARGET ASSEMBLY
Universal Coupling
Side Wall
Counter
Rubber Universal
Stainless Steel Shaft
O-ring Seals
Crank
PLAN VIEW
Universal Coupling
Gear
Targets
10-32 tap
10-32 clear
Spur Gear
SIDE VIEW

Fig.12.

(d) Ion Source Box Extension and Proton Pipe

In order to bring the extracted proton beam out of the cyclotron vacuum chamber, it was necessary to enlarge the hole in the side wall through which the ion source passes (Fig. 13). In addition, an extension was built onto the ion source box which contained a side port through which the beam emerges. The extension consists of a $13\frac{1}{2}$" square by 6" deep box of $\frac{3}{8}$" brass sealed to the side wall of the cyclotron by a flat rubber gasket. A hand-operated vacuum gate covers a 2" diameter port on the exit side of the extension box (see Fig. 13). When the gate is open, the pumping system of the cyclotron also evacuates the pipe for the external beam. The absence of a solid window eliminates all unnecessary scattering of the beam.

The beam moves across the room in a 4" copper pipe which is terminated at each end by a 12" section of copper bellows to give one a range of adjustments. The stretched current-carrying wire technique was employed to study the path of the beam after it leaves the cyclotron. It was found that the beam would not deviate more than 0.16" from a straight line drawn from 9" outside the exit port to the entrance of the deflection magnet.

ION SOURCE BOX EXTENSION

PLAN VIEW

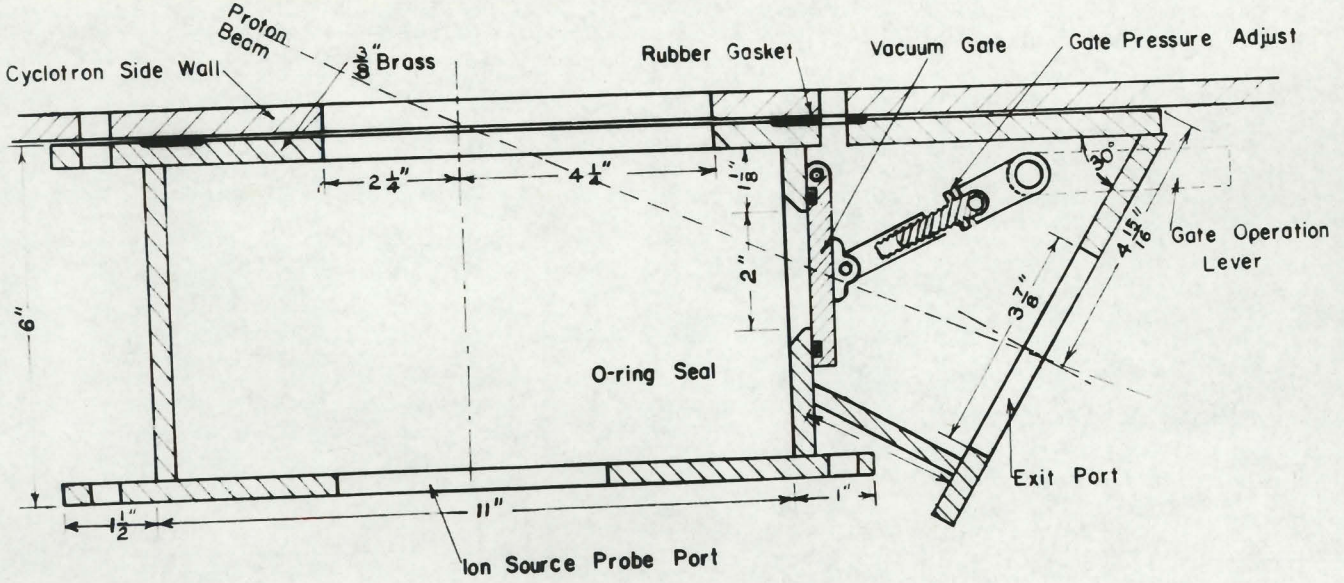

Fig.13.

C. Extraction and Measurement of the External Beam

(1) Methods of Beam Measurement

(a) General Discussion

A number of methods were employed to measure the external beam of the cyclotron.

The Faraday cup is probably the most straightforward means of measurement. It is essentially a metal block sufficiently thick to stop the protons which is placed in the proton beam. The charge collected in the block is measured. Since the output from the Faraday cup is of the order of 10^{-11} amps, a sensitive direct current amplifier must be used to detect it.

If only a qualitative measurement of the beam is desired, such as its cross-sectional shape, position, and intensity distribution, X-ray plates are satisfactory. Glass plates are also darkened by bombardment with protons.

As a check on the beam current measured with the Faraday cup, the beam intensity was also determined using the well-known cross-section for the C^{12} (p, pn) C^{11} reaction.

(b) Direct Current Amplifier and Integrator

A sensitive direct current amplifier was designed and constructed to measure the proton current from the Faraday cup (Fig. 14). The circuit employs a high gain tetrode electrometer tube (the Raytheon CK5886) which measures the voltage drop across one of the input resistors (10^9 to 10^{12} ohms). The signal, amplified

D. C. AMPLIFIER AND CURRENT INTEGRATOR

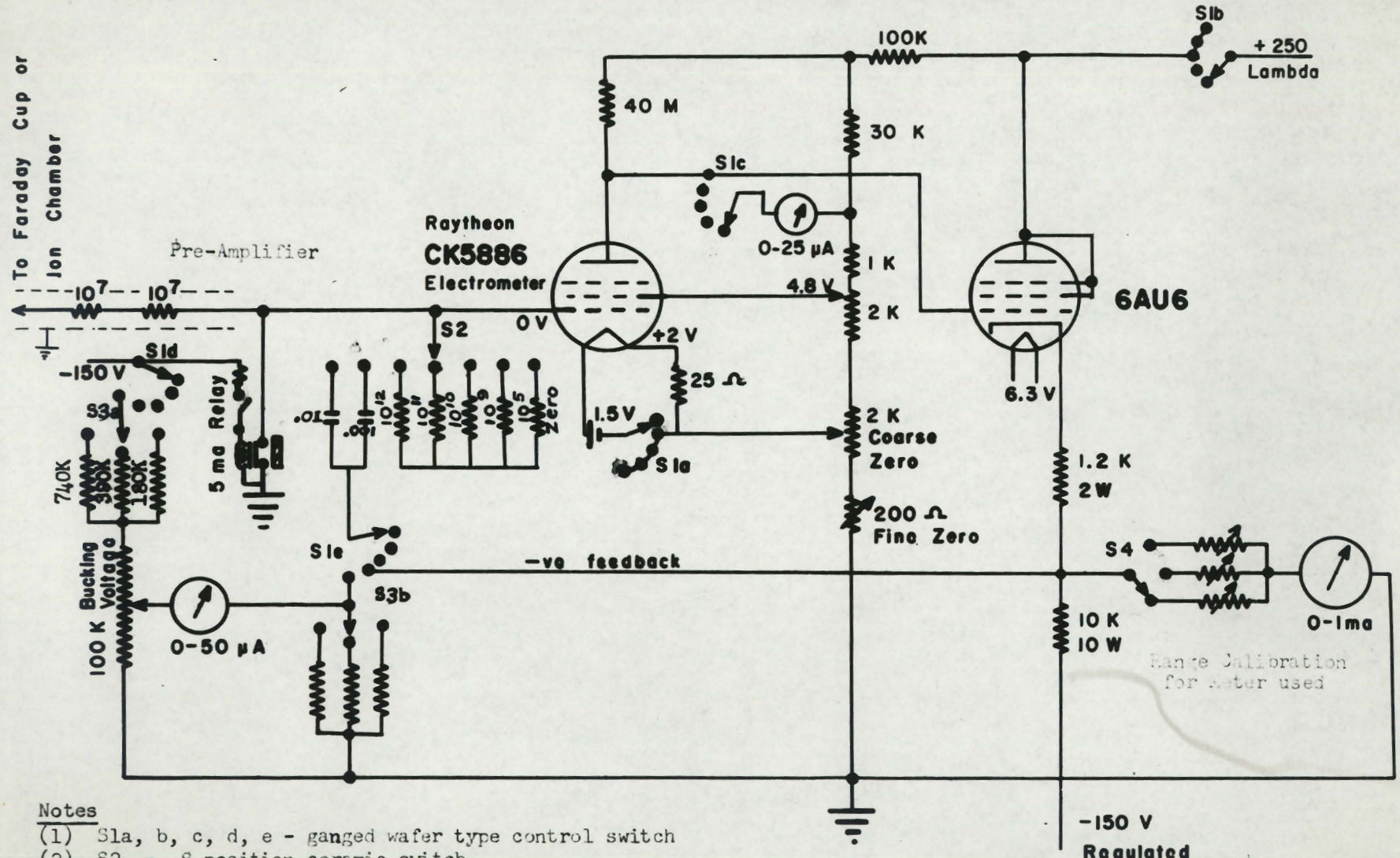

Notes

(1) S1a, b, c, d, e - ganged wafer type control switch
(2) S2 - 8 position ceramic switch
(3) S3a, b - ganged range switch for integrator
(4) .01 and .001 mfd integration capacitors-polystyrene.
(5) 10^{12}, 10^{11}, 10^{10} ohm resistors - Victoreen
10^9 - S.S. White

Fig.14.

150 times by the electrometer tube, is fed onto a 6AU6 cathode follower, which drives a millimeter. On maximum sensitivity, the meter will read full scale for a collected current of 10^{-13} amps. Ninety per cent of the signal is fed back to the input. This reduces the voltage gain in the circuit to almost unity, but greatly improves its linearity and stability. The negative feedback also reduces the input time constant as the inverse of the loop gain.

$$\tau_f = \frac{\tau_o}{1+\beta A}$$

Where β is the feedback factor and A is the gain.

The electrometer tube and associated resistors, condensers, and switches were mounted in a separate pre-amplifier chassis. This enabled one to keep the lead from the detector to the electrometer short, minimizing the input capacitance and radio frequency pickup. The electrometer was covered with 5 turns of 0.01 in. μ-metal and $\frac{1}{8}$" of soft iron so the pre-amplifier might be operated in magnetic fields. No effect on the amplification was observed when the pre-amplifier was moved to a position 3 ft from the cyclotron magnet coil. Radio frequency pickup was satisfactorily removed from the signal lead by inserting two 22 megohm resistors which act as series filters.

Scattered radiation about the room was found to produce an ionization current of about 10^{-12} amps in the pre-amplifier. Shielding the chassis with 2" of lead bricks had little effect,

so the whole pre-amplifier was placed in an evacuated chamber. This reduced the effect to a negligible value.

The circuit was designed to operate from +250 and -150 volt regulated power supplies. For stability, it is necessary to operate the heater of the electrometer tube from a 1.5 volt dry cell. Further details of the circuit may be seen in Fig. It should be noted that the electrometer should not be operated at a plate voltage of over +15 volts or the grid current will become excessive.

Current Integrator Circuit

For many applications it is advantageous to measure the total charge collected rather than the instantaneous current. Two integrator circuits are provided in the amplifier which measure the charge collected on a polystyrene condenser.

In one circuit, the collecting condenser replaces the input resistor, and the charge collected is read directly from the reading on the amplifier meter. Ploystyrene condensers were used as collectors because of their low leakage rate, and low dielectric absorption. The circuit is zeroed by grounding the condenser through a 5 ma ceramic relay mounted in the pre-amplifier chassis.

The other circuit is designed as a calibration device which should be accurate to within 2 per cent. The electrometer tube acts only as a balancing device, a 10 μa current indicating that the grid is at ground potential. The voltage built up in the polystyrene condenser is bucked out by an opposing voltage, thus

keeping the grid at ground potential. The bucking voltage is accurately determined from the current flowing through a 0-50 μa meter and precision w.w. resistor. Note that the grid should not be allowed to become positive with respect to the cathode, or grid leakage will occur.

This instrument has been in periodic service as an amplifier over a period of a year. It has proven itself fairly stable, with less than 1 per cent/hr drift on the 1 volt range being observed after a 15 minute warm-up period.

(c) The Faraday Cup

The Faraday cup consists of a 3" diameter evacuated cylinder in which is suspended a well insulated brass cup, $1\frac{1}{2}$" deep and $1\frac{1}{2}$" in diameter. To stop all incident protons, the bottom of the cup was made $\frac{3}{4}$" thick. A one thousandth inch dural foil covers the $\frac{7}{8}$" diameter window in the front of the vacuum cylinder. Suspended between the window and the cup is a shielding grid of 0.002" tantalum wire.

If the Faraday cup is to read true proton current, ionization in the surrounding gas must be avoided, and the secondary electron emission greatly reduced. For a high energy proton, a vacuum of better than 20 microns must be maintained in the cup to reduce the ion current to less than 1 per cent." If lower energy protons are being measured, the pressure must be reduced below this in proportion to the rate of energy loss of the protons.

The cup is enough wider than the beam diameter to stop all protons undergoing single coulomb or nuclear scattering of less than

45°. The mean lateral displacement due to multiple scattering is less than $\frac{1}{16}$" as shown by glass plates darkened in the beam. Assuming a gaussian distribution for the lateral displacement, 99.9 per cent of the protons will be stopped within the cup boundaries.

Secondary electrons emitted from the Faraday cup or surrounding surfaces may cause errors in the measured proton current. Most of these electrons have only an energy of a few electron volts so they may be attracted back to the emitting surface by a small positive voltage gradient. A transverse magnetic field of about 100 gauss from a large magnetron magnet was produced across the cup. This is sufficient to stop the escape of electrons with energies less than 1000 electron volts. The $\frac{3}{4}$" deep rim of the cup prevents electrons from escaping along the magnetic flux lines.

An investigation was made into the variation of the cup reading with changes in the magnetic field, pressure, and screen voltage. The current was reduced by 40 per cent when the magnetic field was removed. A large variation in the current collected is noted if the pressure rises above 1 mm Hg due to the ionization in the surrounding gas.

The voltage applied to the screen has a very marked effect on the current collected, (Fig. 15). The original screen of 0.001" Al foil was replaced with a wire grid of 0.002" tantalum wire spaced at 0.1" intervals to cut down the secondary emission from the screen. In addition, the cup rim was increased from $\frac{1}{4}$" to $\frac{3}{4}$" deep, but little

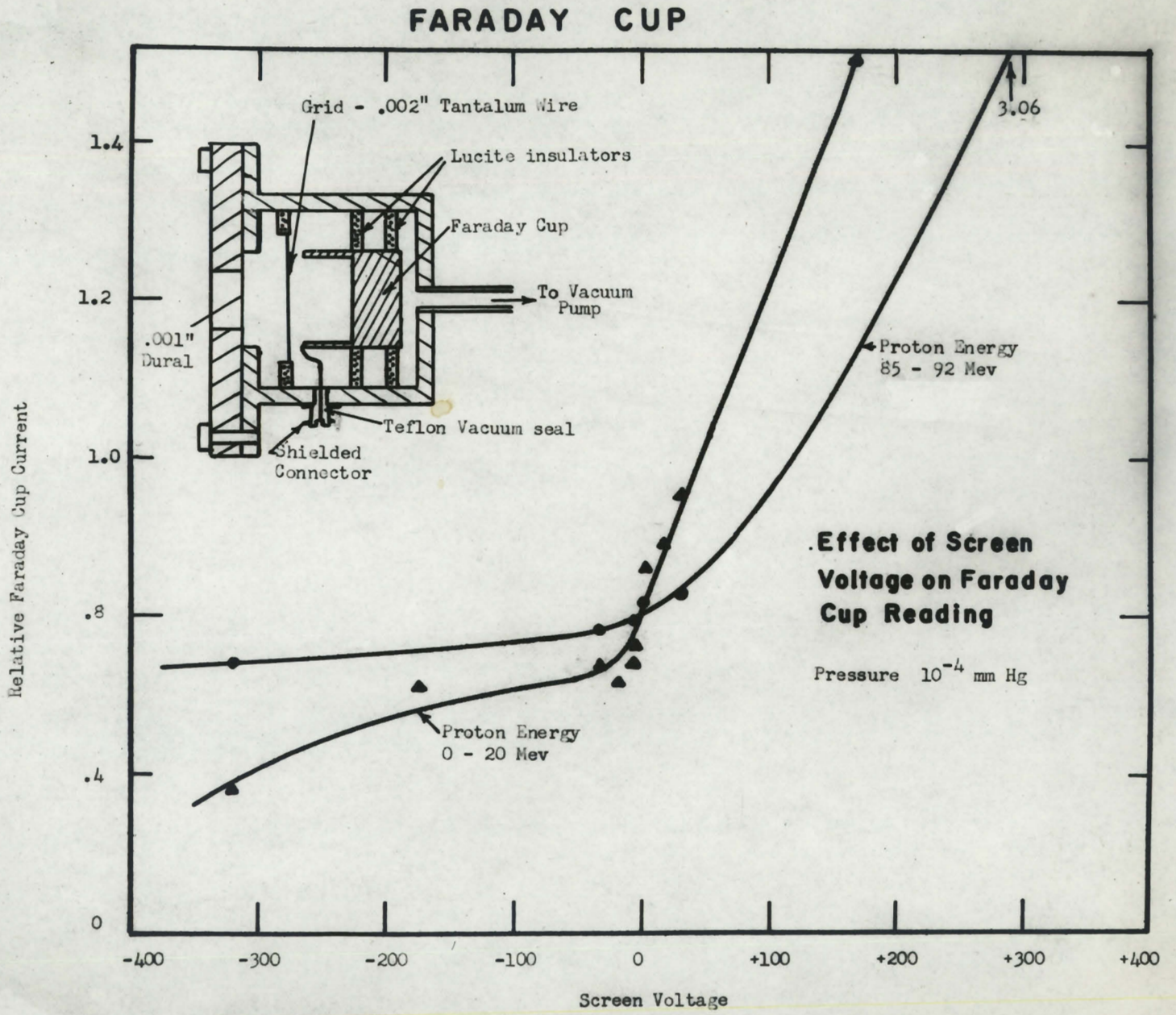
FARADAY CUP
Grid - .002" Tantalum Wire
Lucite insulators
Faraday Cup
To Vacuum Pump
.001" Dural
Teflon Vacuum seal
Shielded Connector
3.06
Proton Energy 85 - 92 Mev
Effect of Screen Voltage on Faraday Cup Reading
Pressure 10^{-4} mm Hg
Proton Energy 0 - 20 Mev
Relative Faraday Cup Current
1.4
1.2
1.0
.8
.4
0
-400
-300
-200
-100
0
+100
+200
+300
+400
Screen Voltage

Fig.15.

improvement was observed. The effect is most noticeable when low energy protons are being collected, as shown in Fig. The most consistent results will be attained by operating the cup with -50 volts on the screen.

(d) X-ray Plates

X-ray plates were used in order to determine the shape and position of the beam. Exposures of from 0.1 to 10 seconds were used, depending upon the beam density.

An aluminum plate holder was constructed which mounted on the main probe. This enabled one to determine the distribution of the beam in the gap between the third and fourth channel sections. In addition, an apparatus was built which can slip a plate in endwise through the vacuum port on the ion source extension without disturbing the main vacuum. A pair of movable rods passing through O-ring seals move the plate and swing it out into the beam.

(e) Glass Plate Technique

Protons decelerated in glass produce a dark stain along their paths. This method has the advantage that the resultant picture is obtained immediately, with no development, and the particle ranges are evident. The plates are darkened sufficiently by exposures of a few seconds in the direct internal beam. These bombardments must be made at low beam current or in short bursts, since heating of the glass destroys the dark stain.

This phenomena was used to obtain the vertical beam heights and energy distributions described in the introduction (Fig. 2).

In addition, a number of plates were stacked together and mounted on the main probe parallel to the beam. These would show the cross-sectional distribution of the beam, and in addition the energies accepted in various parts of the cross section.

(f) Proton Activation of C^{12}

As a check on the Faraday cup, the external beam intensity could be measured from the activity induced in a target whose reaction cross section is well known. One of the best known cross sections is for the C^{12} (p, pn) $C^{11} \xrightarrow[20.5 \text{ min}]{\beta^+} B^{11}$ reaction whose cross section is known to within ± 10 per cent in the energy region of interest.

(2) Beam Extraction

On first trial a proton beam of 4.5×10^{-12} amperes/in^2 intensity was extracted from the cyclotron using the new extraction configuration and orientation. This was much better than had been obtained previously and meant that the channel was in better alignment. This beam was obtained from the 1.04 gm/cm^2 uranium target at a radius of $35\frac{31}{32}$" and an internal cyclotron beam current of 0.7 μa. The yield was found to increase almost threefold when the cyclotron current was increased from 600 to 625 amps as shown in Fig. 16. This increase is probably due to a decrease in the field gradient with higher magnet currents at large radii, which makes it possible for the beam to spiral out to a larger radius before it begins to blow up.

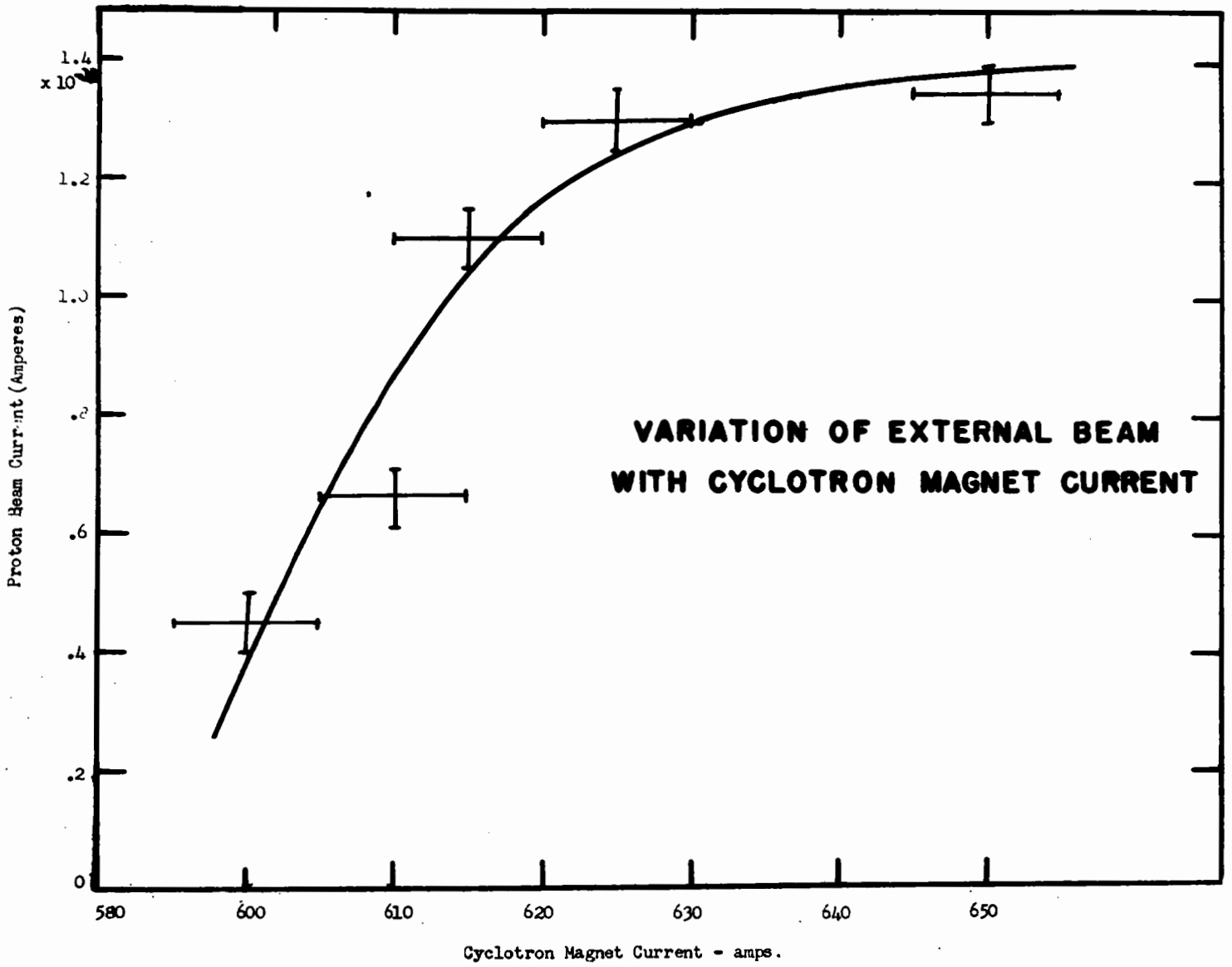
VARIATION OF EXTERNAL BEAM
WITH CYCLOTRON MAGNET CURRENT
Proton Beam Current (Amperes)
x 10
1.4
1.2
1.0
.8
.6
.4
.2
0
580
600
610
620
630
640
650
Cyclotron Magnet Current - amps.

Fig.16.

The external beam was not maximized with the thickest target of 1.04 gm/cm^2 uranium, so the targets were changed to two targets of 0.62 and 1.46 gm/cm^2 and a 2.5 gm/cm^2 tungsten target. A small increase in the maximum beam intensity was obtained with the 1.46 gm/cm^2 target.

(a) Initial Study of the Beam

A number of X-ray plates were taken of the external beam at the exit port and also after it had travelled some distance out from the cyclotron in air. The beam was bending in towards the cyclotron almost 3° more than had been predicted by the wire stretch, and, at that rate, it would have been difficult to bend it through the hole into the corridor. In addition, the emerging beam was being clipped off on the inside edge by the exit port. To bring the beam out faster, either the whole channel could be shifted out slightly, or an extra section added to it. Without shims, the last section of channel decreases the field at 36" by 20 gauss, a negligible amount. A fifth section, being still farther from the centre, needs no shimming. This section of channel was added in conjunction with the beam focusing device attached to the main probe and described in the following section.

At a cyclotron current of 625 amperes without the focusing device, however, two well-defined horizontal lobes of beam appeared at the exit port with a separation of $\frac{1}{2}$". These spread rapidly to a $1\frac{1}{4}$" spacing $2\frac{1}{2}$ feet from the port. This would place the effective origin of the beam only 20" behind the exit port, which seemed to indicate that some strong defocusing force inside the cyclotron was acting on the beam.

(b) Focusing the External Beam

1. External Focusing

If the external beam were not focussed before it entered the deflection magnet, 90 per cent of its intensity would thus be lost. Several types of strong focusing were proposed to retain the beam in a small area. A magnetic quadrupole system employing electromagnets would have been the most effective, but it was rejected because of its high cost.

An electrostatic strong focusing system was suggested and designed by Mr. C. Foster. This system has a calculated focal length of 12 ft when it is operated with a maximum field gradient of 25,000 volts/cm. It consists of four quadrupole sections, each 10" long and comprising of four chromium plated brass electrodes with roughly hyperbolic faces. The strong focusing action is obtained by a 90° rotation in the sense of the voltages applied to successive sections which alternately focus and defocus the protons in two mutually perpendicular planes. The lens could be operated up to a maximum of 17,000 volts in air, at which potential the corona and sparking excessively loaded the r.f. power supply. The complete lens was operated in the external beam, but no noticeable focusing effect was observed.

The sense of the voltages was changed so that the lens focussed only in one plane and defocussed in the other. This would be a practical system since the steering magnet will accept a beam 1" high and 4" wide. The lens now changed the $\frac{3}{4}$" collimated beam into an ellipse from whose eccentricity the focal length was found to

be 8 ft as measured from the centre of the lens. Two such lenses would be able to focus the beam, but over 2/3 of the protons would be lost because of the small entrance aperture of this low power system to such a highly divergent beam.

2. Internal Focusing of Beam

The beam was spreading too quickly to be easily focussed, so the scattered beam inside the cyclotron was carefully studied to determine the reason for this defocusing action. A series of X-ray plates of the beam emerging from the first three channel sections was taken by means of an aluminum plate holder mounted on the main probe. The beam shape is similar to that expected, with high fins on the inner side corresponding to protons in a higher field region which just squeeze through on the inside of the channel (see Fig. 17). The observed lobe structure is probably due to a focusing effect by the distorted lines of flux in the channel. A variation in the cyclotron magnet current produced little change in the beam shape, but a marked change in the intensity.

A stack of glass plates was mounted on the main probe and bombarded in the deflected beam for 20 minutes to give the shape and energy distribution of the beam. Using the range of protons in glass as determined by Dr. J. S. Kirkaldy[8], the maximum energy of the beam is 94 Mev, with no appreciable difference in energy between the inner and outer edges of the beam. The critical region appeared to be just beyond the magnetic channel, so a series of X-ray plates were taken at various distances from the end of the channel. These were inserted through the exit port using the

INTERNAL FOCUSING OF SCATTERED BEAM

No Focusing Wedges

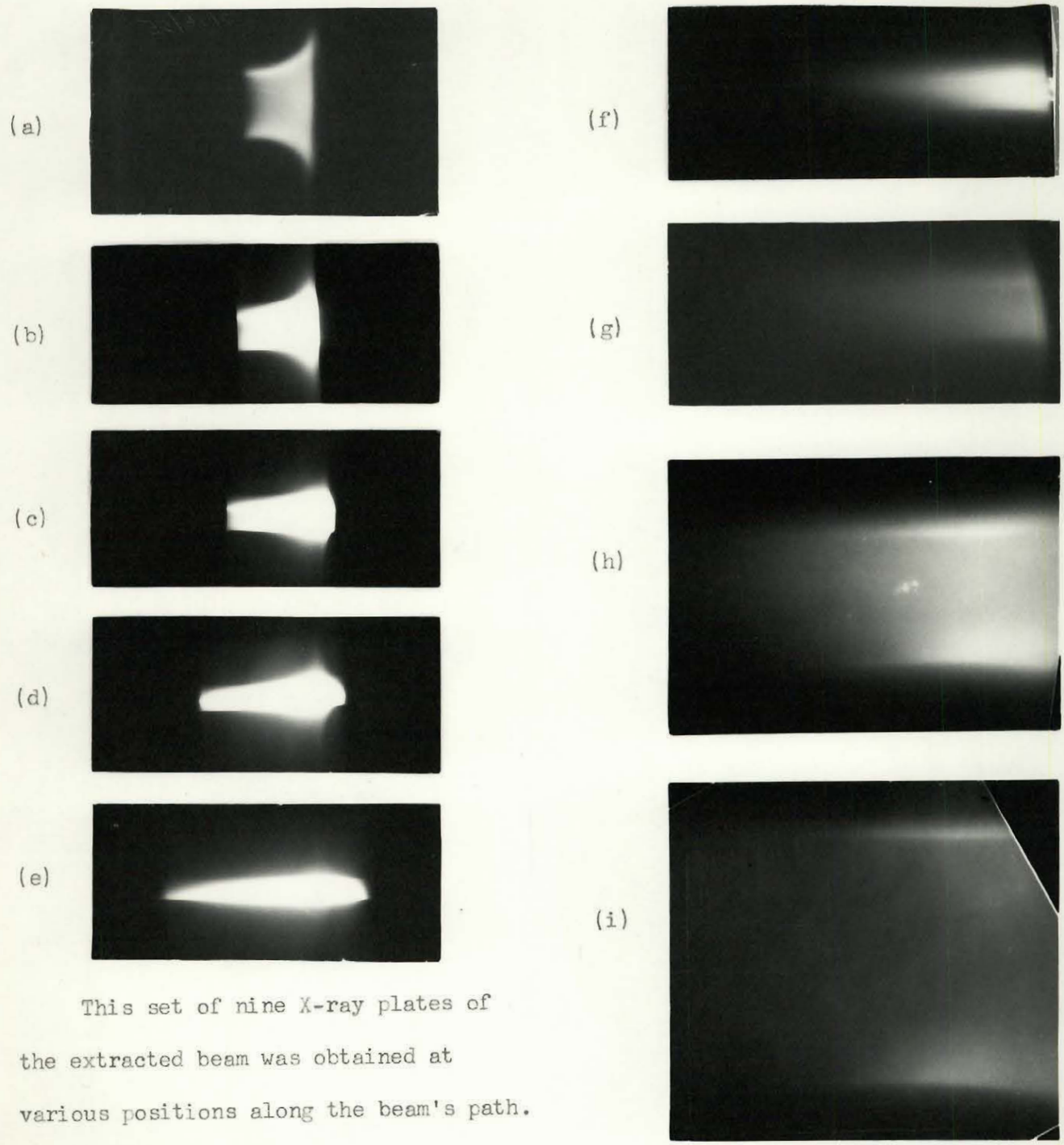

This set of nine X-ray plates of the extracted beam was obtained at various positions along the beam's path. Their relative positions are indicated in Fig.18.

Fig.17.

apparatus described in section D (1) (d) (on page 26). These were compared with plates taken at various positions between the exit port and entrance to the deflection magnet. Fig. 17 is a contact print of this series of plates. Their positions, and the beam focusing which they indicate, are shown in Fig. 18. The beam was highly focussed vertically and defocussed horizontally by fringing fields in the cyclotron and magnetic channel. The vertical focussing is so strong that the beam was brought to a line focus at the point where it passes through the side wall of the cyclotron, and spreads out quickly beyond this point.

Since many of the pertinent parameters are not well known, a good theoretical calculation of this focussing action is rather difficult. An approximate treatment, however, gives one a good concept of the factors involved.

The components of the magnetic field in a current free region of unit permeability are given by

$$\text{Curl } B = 0 \qquad (1)$$

In a region of rotational symmetry, with a field gradient $\frac{dB_z}{dr}$ such as one encounters in the cyclotron, this reduces to

$$\frac{dB_z}{dr} = - \frac{dB_r}{dz} \qquad (2)$$

The field gradient may be assumed to be constant in the vertical plane so

$$B_r = - \left(\frac{dB_z}{dr}\right) z \qquad (3)$$

FOCUSING OF EXTERNAL BEAM

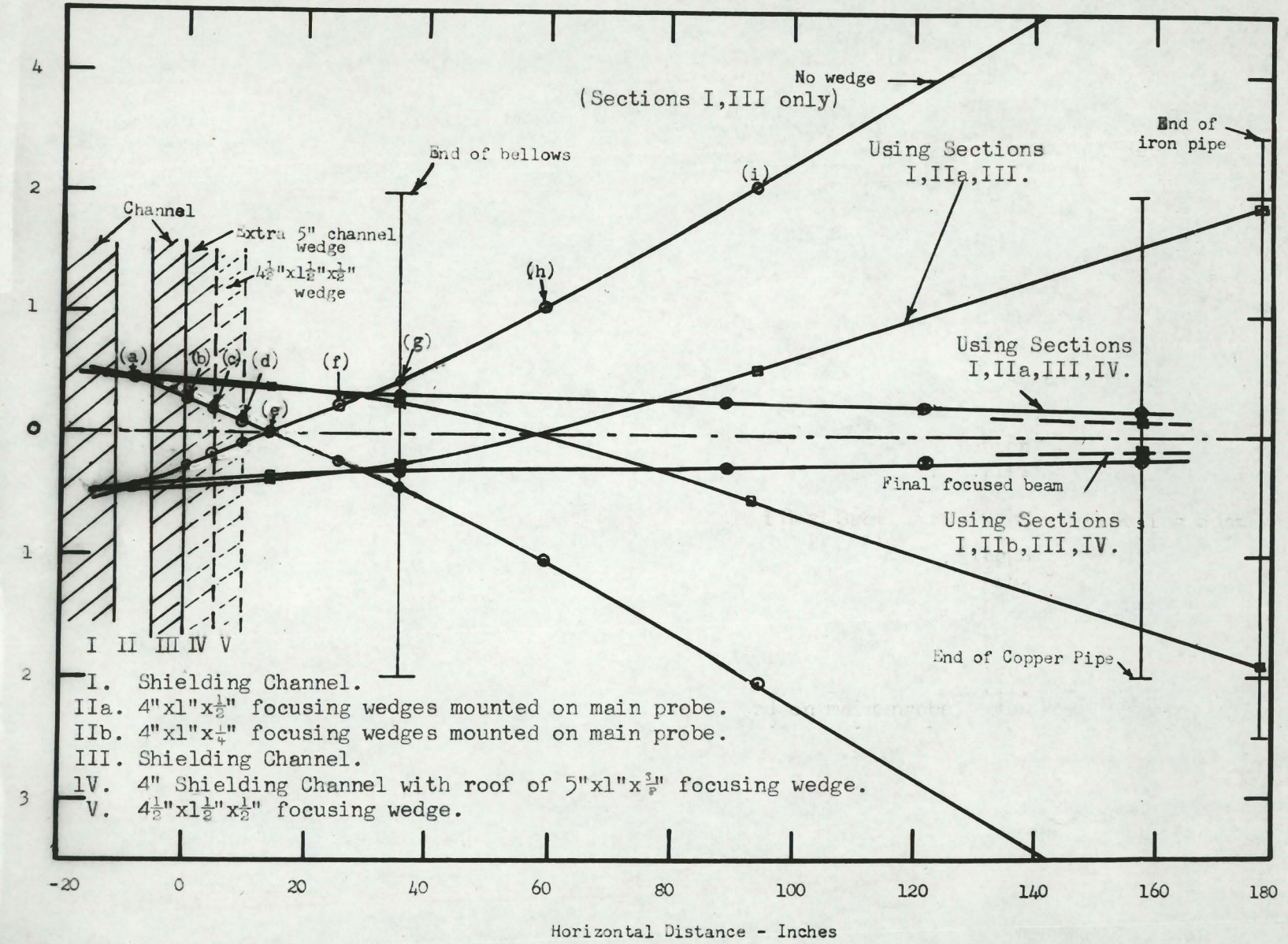

Fig.18.

where z is measured from the central line of symmetry of the cyclotron. The vertical restoring force on a proton is

$$F_z = -e v_T B_r = -e r \omega_o B_r = \frac{e^2 B_z}{m} r B_r \quad (4)$$

for small displacement angles, where v_T is the tangential velocity of the proton, and ω_o its angular velocity around the cyclotron.

Substituting (3) into (4) one obtains

$$F_z = \frac{e^2}{m} r \frac{dB_z}{dr} z = -m \omega_o^2 n z \quad (5)$$

$$\text{where} \quad n = -\frac{r}{B_z} \frac{dB_z}{dr} \quad (6)$$

In a rotationally symmetric field the proton will thus undergo a vertical oscillation of angular frequency

$$\omega_z = \omega_o \sqrt{n} \quad (7)$$

Protons originating from a point will be brought into a line focus in a distance

$$S = \frac{\pi r}{\sqrt{n}} \quad (8)$$

from the source.

If, instead of a rotationally symmetric field, a magnetic perturbation is applied over a short arc of length d, the focal length is

$$f = \frac{r^2}{nd} \quad (9)$$

Neglecting the effect of the channel, the scattered beam will travel in a region with an average n of about 4, so it will be brought

to a line focus a distance of 60" from the scatterer. The focusing distance observed is very close to this (see Fig. 18).

The ideal external beam would be one parallel, or slightly converging. Such a beam could be produced by introducing regions of positive field gradient (negative n) inside the cyclotron tank to nullify the over-focusing negative field gradients along the path of the beam. This defocusing lens must have (to the first approximation) a focal length equal to its distance from the original point of focus. For such a lens mounted on the main probe, this distance is 30". A lens producing an n equal to -10 over a distance of $5\frac{1}{2}$" would be sufficiently powerful to do this.

The field gradient which focuses vertically also defocuses in the horizontal plane, and conversely for the opposite field gradient. Essentially the same situation exists as for the vertical focusing except for the natural 180° focusing action of the field. In a rotationally symmetric field, a scattered proton will return to the central axis in a distance

$$S = \frac{\pi r}{\sqrt{1 - n}} \qquad (10)$$

from the source.[12]

In order to bring the beam into better focus, two negative n lenses were constructed. The one consisted of a pair of Armco iron wedges, 4" long and 1" wide, and increasing from a sharp edge to a width of $\frac{1}{2}$" at the outer edge (see Fig. 19). These were mounted on the main probe straddling the beam, so they could be moved to any radius to adjust the focusing effect. The second set

DETAILS OF MAGNETIC CHANNEL AND FOCUSING WEDGES

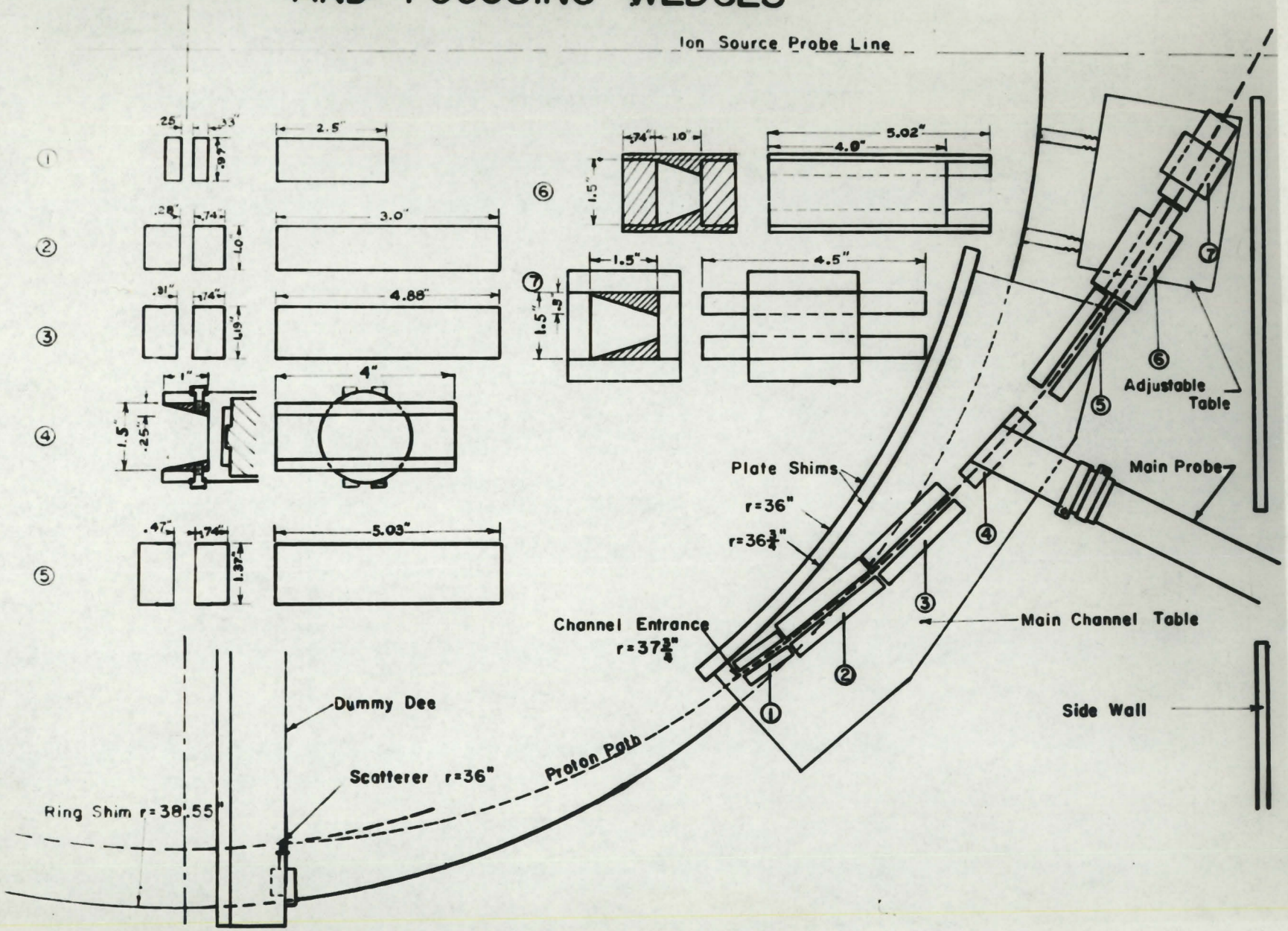

Fig.19.

has the dimensions 5" x 1" x $\frac{3}{8}$", and was mounted on a fifth section of magnetic channel.

Using only the lens on the main probe, the line of focus was moved outward 45". Large distortions in the beam occurred because the field gradient is inhomogeneous over the width of the channel. A weaker lens, 4" x 1" x $\frac{1}{4}$" was made for the main probe, which reduced this distortion. A number of focusing arrangements were tried, the most satisfactory consisting of the 4" x 1" x $\frac{1}{4}$" lens on the main probe used in conjunction with the extra length of channel and a pair of lenses, $4\frac{1}{2}$" x $1\frac{1}{2}$" x $\frac{1}{2}$" beyond this (Fig. 19). This concentrates most of the beam in an area $\frac{1}{4}$" high and 3" wide. at the entrance to the deflection magnet. This size of beam is easily handled by the deflection magnet.

These focusing wedges appear to be a powerful way to concentrate a beam before extraction. Using an appropriate 4 section, strong focusing lens inside the cyclotron, it might be possible to extract a pencil-sized parallel beam.

3. Extracted Beam Intensity

The theoretical extraction efficiency for the system using the 1.46 g/cm^2 target is 1.30×10^{-4}. This includes an 8% correction to the single coulomb scattering to allow for multiply scattered protons.[13]

The extracted beam was measured by two different methods which gave both the beam intensity and its distribution.

(a) Carbon Activation Measurement

The cross-section for the reaction C^{12} (p, pn) $C^{11} \xrightarrow[20.5\ min]{\beta^+} B^{11}$ is well known over a wide energy range.[11,14,15] The 20.5 minute β^+ activity is very free from interfering half-lives, and the two 0.51 Mev annihilation γ-rays are easy to count in a NaI scintillation spectrometer. Six rectangular graphite samples, $\frac{1}{2}" \times \frac{3}{8}" \times \frac{1}{16}"$ were placed in a tight row at the exit port. Their alignment was first checked by X-ray plates; it is estimated that 95 per cent of the extracted beam hit the targets. A seventh sample was placed just outside the beam to act as a monitor for scattered protons, and to detect neutron-induced activity. The samples were bombarded for 20 minutes with an average internal cyclotron beam of 0.52 μa; 625 amperes magnet current; and the 1.43 gm/cm^2 uranium target placed at a radius of $35\frac{31}{32}"$.

The activity was determined by separately counting the annihilation radiation of each sample on a NaI (Th) scintillation spectrometer. The photomultiplier pulses were fed into the 28 channel kicksorter, which counted the 0.511 Mev annihilation radiation in 3 channels. The 6 samples in the beam all showed an appreciable activity above background, while the seventh placed outside the beam showed no measurable counting rate. Counting was carried out over five half lives; all samples showed a clean 20.5 minute activity.

The efficiency of the counting system had been carefully determined previously with sources calibrated in a 4π β-counter.[16]

With the source positioned 3.7 cm from the face of the $1\frac{1}{2}$" by $1\frac{1}{2}$" cylindrical crystal, the efficiency is 0.0084 ± .0008. The reaction cross-section at 85 Mev is 68.5 ± 6 millibarns.

The rate of formation of C^{11} nuclei, $\frac{dN}{dt}$ for a 20 minute bombardment time T_B is given by

$$\frac{dN}{dt} = \frac{R_t}{2} \times \frac{T_{\frac{1}{2}}}{.693} \times \frac{1}{T_B} \qquad (1)$$

R_t is the true counting rate at half bombardment time. It is corrected for the finite time of bombardment. This correction is

$$\frac{R_{true}}{R_{apparent}} = \frac{\lambda T_B}{2 \sinh \frac{\lambda T_B}{2}} = 0.982. \quad (2)$$

The factor 2 in the denominator of equation (1) is to account for the two annihilation γ-rays.

The incident proton current on a graphite target of thickness t gms/cm^2 is

$$I_p = \frac{\text{Rate of formation of } C^{11}}{\text{Probability of Interaction}}$$

$$I_p = 4.72 \times 10^{-17} \frac{dN}{dt} \times \frac{1}{d} \text{ amperes}$$

where d is the target thickness in gms/cm^2.

The current distribution measured by this method is shown in Fig.*20*. The integrated current is 4.6 ± .8 x 10^{-11} amperes per microamp of internal cyclotron current.

The extraction efficiency for the system is 0.87 x 10^{-4} which compares favourably with the theoretical efficiency of 1.3 x 10^{-4}.

PROTON BEAM PROFILES

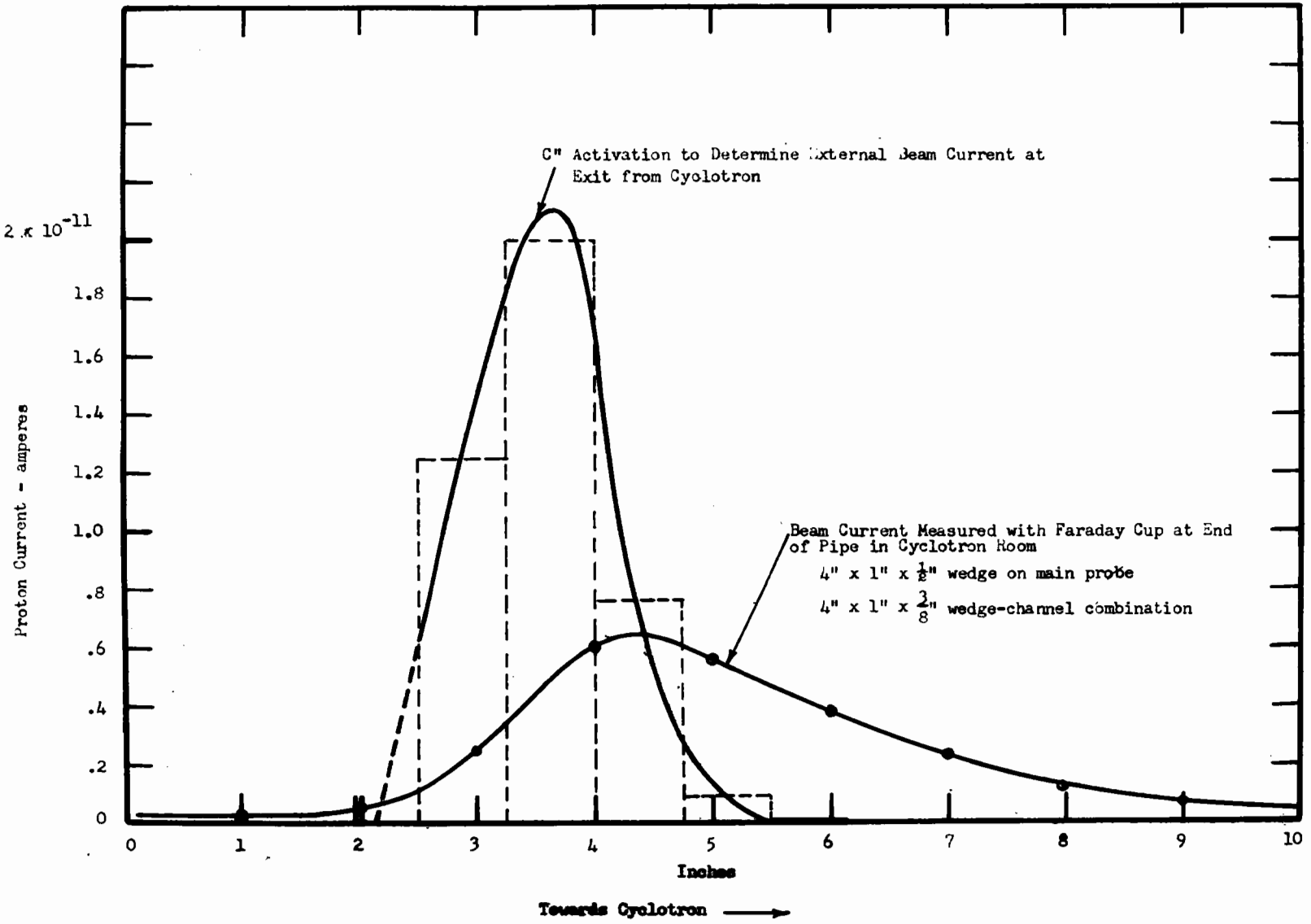

Fig.20.

(b) Faraday Cup Measurements

A second measurement of the beam distribution was made with the Faraday cup at the end of the evaduated pipe in the cyclotron room. It is compared with the distribution at the exit port in Fig. 20 The intensity of the extracted beam may change by a factor of 30 per cent or more in a one minute period. In order to obtain quick readings without shutting off the beam, a selsyn-driven trolley was constructed to move the Faraday cup horizontally across the beam. This system could not be operated in the fringing field of the cyclotron, so a direct comparison with the carbon activation determination could not be made. This distribution applies when the focusing system consists of the 4" x 1" x $\frac{1}{2}$" wedge on the main probe in conjunction with the 4" x 1" x $\frac{3}{8}$" channel-wedge combination. This focusing system has been improved since then, so that a more concentrated beam is now obtained.

A pair of X-ray plates were taken, inside and outside the Faraday cup, to show what fraction of the beam was actually seen through its $\frac{7}{8}$" aperture window. A suitable correction was applied by estimating the area of the beam which did not enter the cup. The total current was calculated to be $2.4 \pm .5 \times 10^{-11}$ amperes for a 10 cm beam, or $4.37 \quad .9 \times 10^{-11}$ amperes per microamp of internal cyclotron beam; this is only half the value given by the carbon activation experiment. The focusing system employed at the time had large aberrations which may have defocused part of the beam. A Faraday cup survey, 4 ft from the exit port, indicated that there was a 15 per cent low energy component of the beam which had probably

passed through the $\frac{3}{8}$" brass side on the ion-source box, and was subsequently bent in toward the cyclotron. This would explain part of the discrepancy between the two measurements.

D. Double Focusing Deflection Magnet

A double focusing deflection magnet was constructed to bend the beam through the 11 ft shielding wall into the cyclotron corridor. This deflection removes all the neutrons and low energy scattered particles from the beam, and conveys it into a low background region which is ideal for counting. The hole through the wall points away from the cyclotron, so that no particles or radiations produced inside the cyclotron tank may directly follow the deflected beam's path.

(1) Theory

(a) Double Focusing of Charged Particles with Sector-Shaped Magnetic Fields

Double focusing sector-shaped magnets have been treated theoretically by Camac[17] and by Cross.[18] First order focusing is obtained in the horizontal plane by presenting different path lengths in the magnetic field to the components of the divergent beam. Particles not entering or leaving the sector perpendicular to its boundaries undergo a vertical focusing or defocusing action due to the horizontal component of the fringing field. By suitably adjusting the angles of entrance and exit, it is possible to obtain both horizontal and vertical focusing for a monoenergetic beam.

The general analytical solution is given in Appendix I for the focusing of a point source into a point image. The equations are:

$$\operatorname{Tan} \epsilon_2 = \tfrac{1}{2}\left[\operatorname{Tan}(\phi - \psi) + \frac{1}{\phi - \cot\eta}\right] \qquad (9)$$

and $$\frac{1}{\ell_d''} = \frac{1}{2}\left[\text{Tan}\,(\phi - \psi) - \frac{1}{\phi - \cot\eta}\right] \qquad (10)$$

where

$$\text{Tan}\,\psi = \text{Tan}\,\epsilon_1 + \frac{1}{\ell'} \qquad (11)$$

$$\text{Tan}\,\eta = \text{Tan}\,\epsilon_1 - \frac{1}{\ell'} \quad . \qquad (12)$$

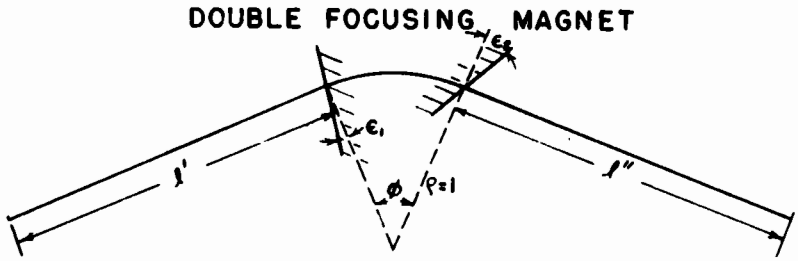

Fig.21.

The magnet is designed to bend the protons through an angle ϕ of 44° with a radius of curvature $\rho_o = 40"$. The object distance l', measured from the scatterer, and the image distance l" from the magnet to the focal point in the corridor, are 14'8" and 12'9" respectively. For these conditions the sector angles were calculated by successive approximations to be $\epsilon_1 = 28.0^\circ$

$\epsilon_2 = -7.9^\circ$.

The astigmatic focusing of the extracted beam in the cyclotron's field will result in different object distances for the horizontal and vertical planes. For this situation, equations (9) and (10) for double focusing remain unaltered, but $l' = l'_v$ is no longer substituted into the associated equations (7) and (8) (see Appendix I). Provided the vertical object plane does not occur too close to the magnet (greater than 150" beyond the deflection magnet) it is possible to regain the double focusing by suitable adjustment of the angles ϵ_1 and ϵ_2.

(b) Energy Resolution

The equations for the dispersion of the magnet are developed in Appendix I (b). The lateral spread of the beam in the corridor, for an unresolved beam entering the deflection magnet, is

$$x \doteq \frac{d\rho}{\rho_o} \left\{ \rho - l'' \tan \epsilon_2 (1 - \cos \phi) + l'' \sin \phi \right\}$$

where $\frac{d\rho}{\rho_o}$ is the fractional spread in momentum.

Putting in the physical values, the spread becomes

$$x = 10.30 \frac{d\rho}{\rho_o} \text{ inches.}$$

Assuming a 4 Mev. energy spread for the extracted beam, the lateral spread in the corridor will be 2.5".

The fringing field of the cyclotron will disperse the beam in the opposite sense to that of the steering magnet. This will decrease the overall energy dispersion of the system. Moreover, since the energies will already be resolved before entering the deflection magnet, appropriate sector angles or field gradients will bring them all to the same focus.

2. Magnetic and Electrical Design

(a) General Considerations

In order to produce the desired magnetic field over the path length of the proton with a minimum of waste flux, a magnet with long, narrow, curving pole-pieces is necessary. A cyclotron type electromagnet with the coils immediately above and below the air gap is the most efficient system, but it is only well suited for cylindrical or nearly cylindrical fields, unless cores with an oblong cross-section are employed. Such coils are more difficult and costly to construct than cylindrical ones. If the coils are moved to the outside yokes, the leakage flux is greater, but any shape of pole-pieces may be used. A single yoked magnet was chosen in preference to one with a double yoke because its power consumption is smaller by a factor of almost $1/\sqrt{2}$.

(b) Magnetic Flux Calculations

A field strength of 1.4 Webers/m^2 must be produced between the pole faces in order to bend a 92 Mev proton through an arc with a radius of 40". The width of usable flux in the field segment should be $3\frac{3}{4}$" to accept all protons emerging from the pipe. A safe design criteria is to maintain a buffer field, equal in width to the air gap, on either side of the deflecting field to allow for edge effects. Hence, the field segments were designed with an average width of $6\frac{3}{4}$" which gives an overall area for the pole-pieces of 210 $in.^2$

The total magnetic flux produced in the air gap for a given magnetizing force depends on the size of the gap, the flux leakage,

and the reluctance of the iron circuit. The leakage flux in this type of a magnet is quite large, and its calculation is at best only approximate. A method of estimating the leakage flux is given in "Magnetic Circuits and Transformers" page 75. The effective area of the air gap is found by adding 2d (d = gap width) onto all the dimensions of the pole-pieces. This increases the area to 325 in^2 which corresponds to a leakage coefficient of 1.55.

The magnetizing force $\mathcal{H}$ required is

$$\mathcal{H} = \oint H \cdot dl.$$

For a series magnetic circuit this becomes

$$\mathcal{H} = \Sigma_i \frac{l_i \phi_i}{\mu_o \mu_i A_i} = \Sigma_i \frac{l_i B_i}{\mu_o \mu_i}$$

In M.K.S. units, $\mathcal{H}$ is measured in ampere turns, ϕ is the total flux in webers, l is the path length in meters, μ_o is the permeability of free space = $4\pi \times 10^{-7}$ henries/meter and μ_i is the permeability of the material relative to free space.

Table I

Component	Flux Density Webers/m^2	μ	Area in^2	Length		mmf. ampere turns
				in	meters	
Air Gap	1.4	1	325	1.5	0.0381	42,300
	1.4	1		1.0	0.0254	28,200
Iron	1.7	310	268	52	1.32	4,700
	1.8	180	254			10,400
	1.9	110	240			18,200
	2.0	68	228			30,700
	2.1	48	217			45,800

Using a working flux density for the Armco iron of 1.8 webers/m^2, the iron should have a cross-sectional area of 254 in^2 The total magnetizing force for the magnet would then need to be approximately 53,000 ampere turns.

A special order of Armco iron was obtained, the pieces being cold-rolled and annealed for maximum permeability. The details of the magnet may be seen in Fig.22&23 In order to make full use of the vertical air gap, the pole-pieces are split into two sections. The $\frac{1}{2}$" thick iron inner pole-pieces also serve as the faces of the vacuum chamber through which the beam passes. A $\frac{1}{8}$" shimming gap between the sections of the pole-pieces enables one to adjust the field distribution in the gap. A second $\frac{1}{8}$" gap between the $4\frac{1}{2}$" feeder-pieces serves as a coarse control to feed field to the outer edges of the air gap.

The 18" diameter central core of the coil has a cross-sectional area of 254 in^2 while the main feeder-pieces are 272 in^2 in area. The surfaces in contact are ground to a 50 millionth inch finish.

The pole-pieces are drawn together with a force of 8 tons by the magnetic field. The four 1" bolts used to attach the feeder-pole-pieces to the cylindrical core will hold up to 16 tons force with safety.

(c) Excitation coil

(i) Wire Specifications

A direct durrent motor generator set rated at 7.5 Kw (65 amperes

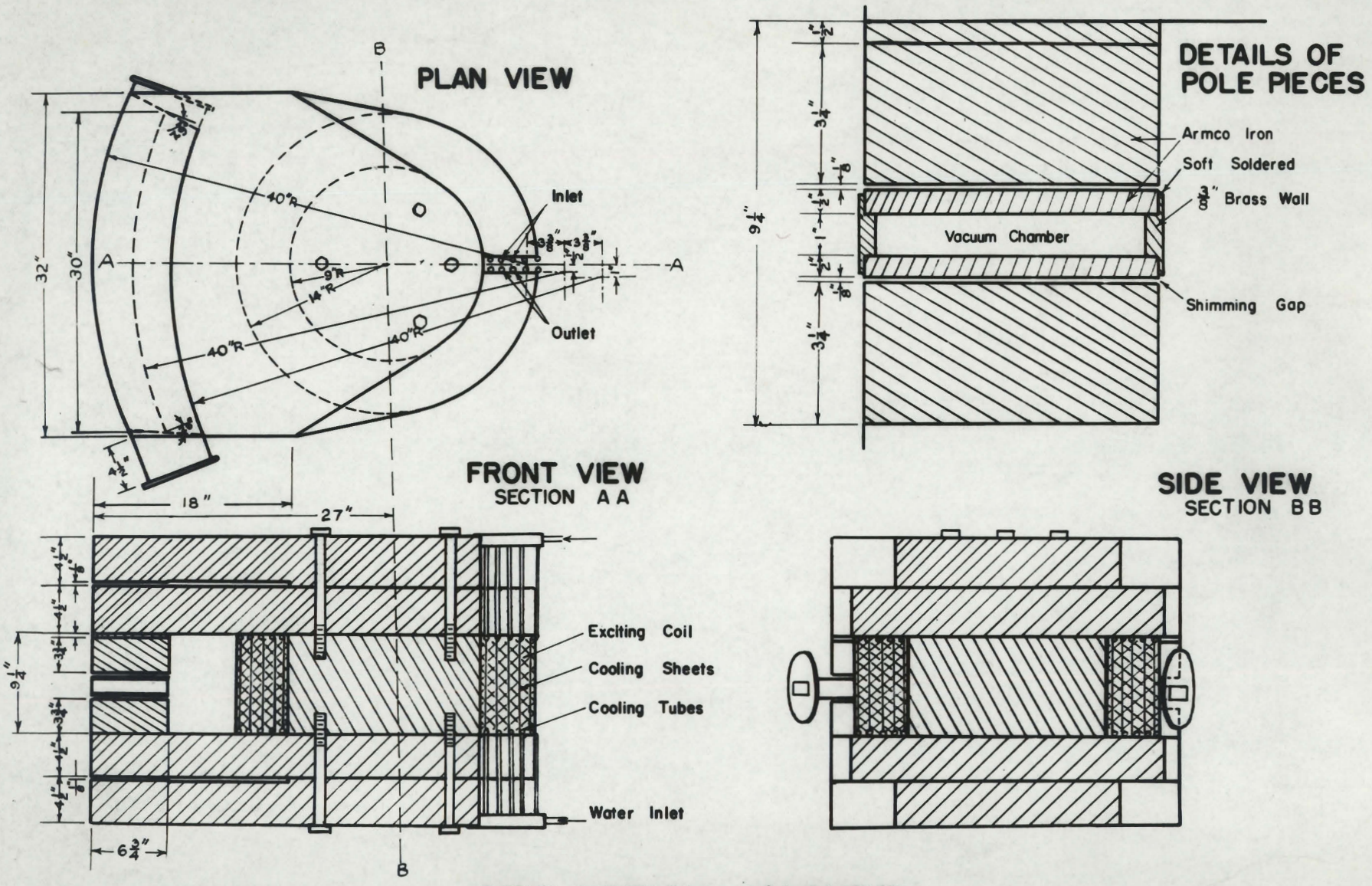

DEFLECTION MAGNET

Fig.22.

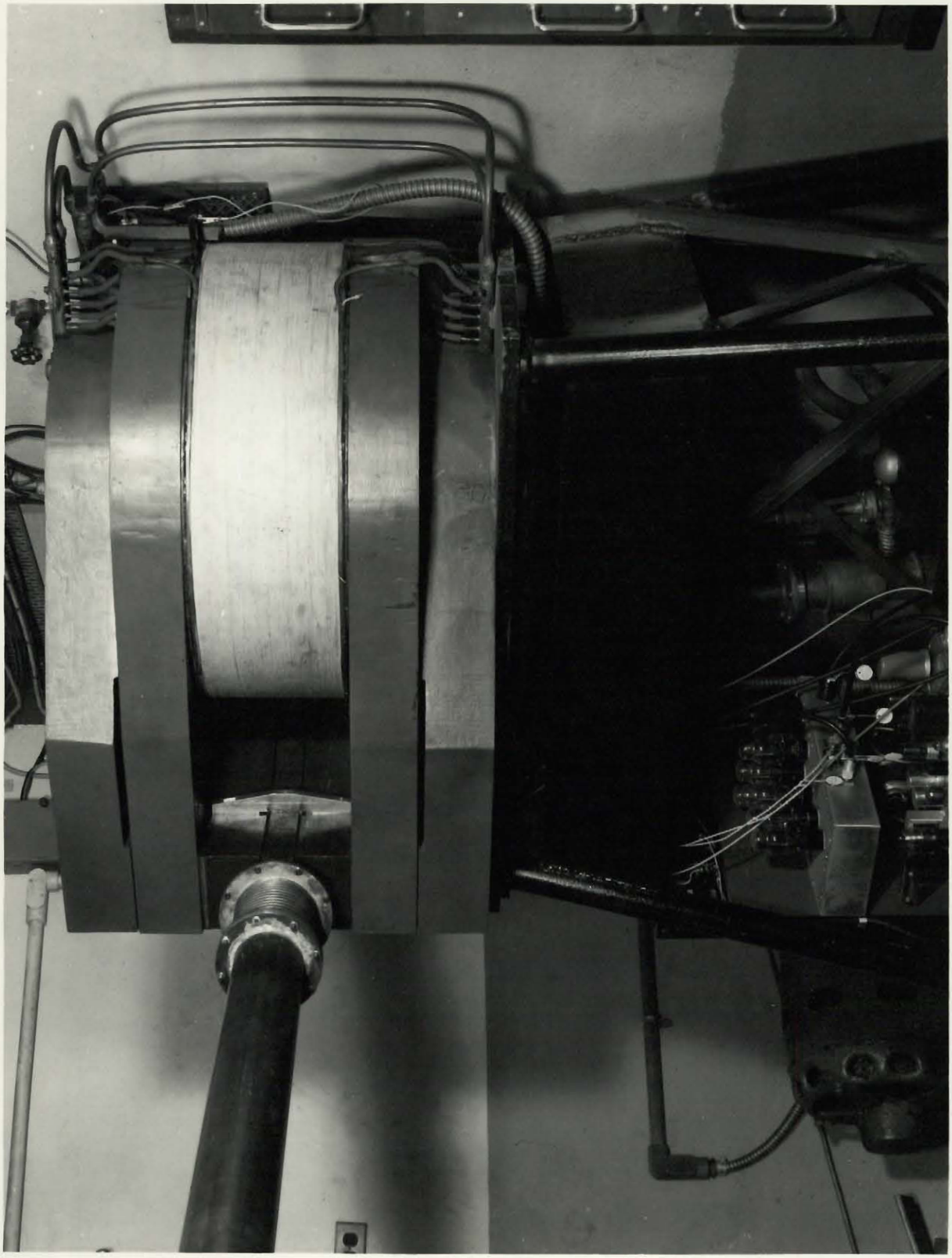

Fig.23.

at 115 volts) was purchased to produce the 53,000 ampere turns field excitation. If the excitation, mean coil diameter ($\bar{D}$ = 23") and voltage (V = 105 volts) are fixed, the resistance per unit length of the wire may be calculated from

$$r = \frac{V}{(NI)\ (\pi \bar{D})}$$

$$= 0.33 \text{ ohms/1000 ft.}$$

This is the resistance of an annealed copper wire of 0.030 in^2 cross section at 75°C.

The final coil specifications were for 950 turns of 0.30" x 0.10" rectangular double cotton covered magnet wire, 6,000 ft in length, and weighing 700 pounds.

(ii) Cooling

The maximum heat dissipation of the coil is 7.5 Kw or 18,000 calories/second. The coil is cooled by $\frac{1}{32}$" copper sheets wrapped around the coil windings every nine layers (approximately every inch). Water flowing through copper cooling tubes soldered to the peripheries of these sheets carries the heat away. A phenol plastic filling compound, sold by General Electric under the code name CG 1008, was used to fill in the voids in the coil and thus improve the heat conductivity. The coefficient of conductivity of the whole coil is estimated to be 1/100 the conductivity of copper. On this basis the maximum temperature rise in the inner layers of the coil would be 40°C with a total flow of 0.2 litres/second in the cooling coils.

A Bernouli-type mercury manometer flow-gauge was constructed to register the flow rate for the cooling water. Adjustable contacts operate neon lights on the cyclotron control panel to indicate the water flow rate.

(iii) Construction of the Coil

The coil was wound on the 28" lathe in the Radiation Laboratory machine shop. The $\frac{1}{8}$" iron winding spool was covered with a double layer of varnished linen cloth for insulation. This did not prove very satisfactory as the solvent from the filling compound drastically decreased its insulating properties, and the linen tended to char in the baking process. Each copper cooling sheet is insulated from ground to minimize the danger of coil damage caused by the development of local shorts. The filling compound must be baked at temperatures up to 120°C to distill off the solvent and improve its insulating properties. An attempt to bake the coil by passing current through it proved unsatisfactory as shorts developed. The baking was completed by heating the whole magnet with a battery of bunsen burners. The shorts were removed by inserting mica sheets between the coil and the iron winding spool.

(d) Magnetic Flux Measurements

The magnetic flux between the pole-pieces was measured with the flux integration instrument. With 60 amperes flowing through the coil and all shimming gaps filled, the magnet was highly saturated with a field of 1.0 webers/m^2, which is some 30 per cent low. Apparently the estimated leakage coefficient was much too low, and

the central core was saturating. These results indicate that a leakage coefficient of 1.9 should have been used. Unless one replaced the central core by a more permeable material such as cobalt iron, the only reasonable alternative was to decrease the gap width. The reduction of the gap width to 1" reduces the leakage coefficient to 1.6, so sufficient field would be available across the gap.

The gap was reduced by closing the vacuum chamber by $\frac{1}{2}$", and inserting a $\frac{1}{2}$" iron plate into the upper pole piece as shown in Fig. 1 . The field is now excited according to the saturation curve of Fig. 24. The flux is quite uniform over the gap, a maximum variation of 3 per cent occuring along the median line to within 2" of either end. Laterally, over a 5" width, the maximum variation is less than $\frac{1}{2}$ per cent. The strength of the magnetic field was checked with a wire stretch and was found to be satisfactory, but with little flux to spare.

3. Magnet Regulation

(a) Necessity for Regulation

The steering magnet will focus the beam on a target some 12 feet distant. In order to keep the portion of the beam being observed steady to within 0.1", a flux regulation factor $\phi/\Delta\phi$ of 1000 is necessary. Neglecting the saturation of the magnet, this corresponds to a maximum current variation of 0.06 amperes.

The possible current fluctuations which must be removed are as

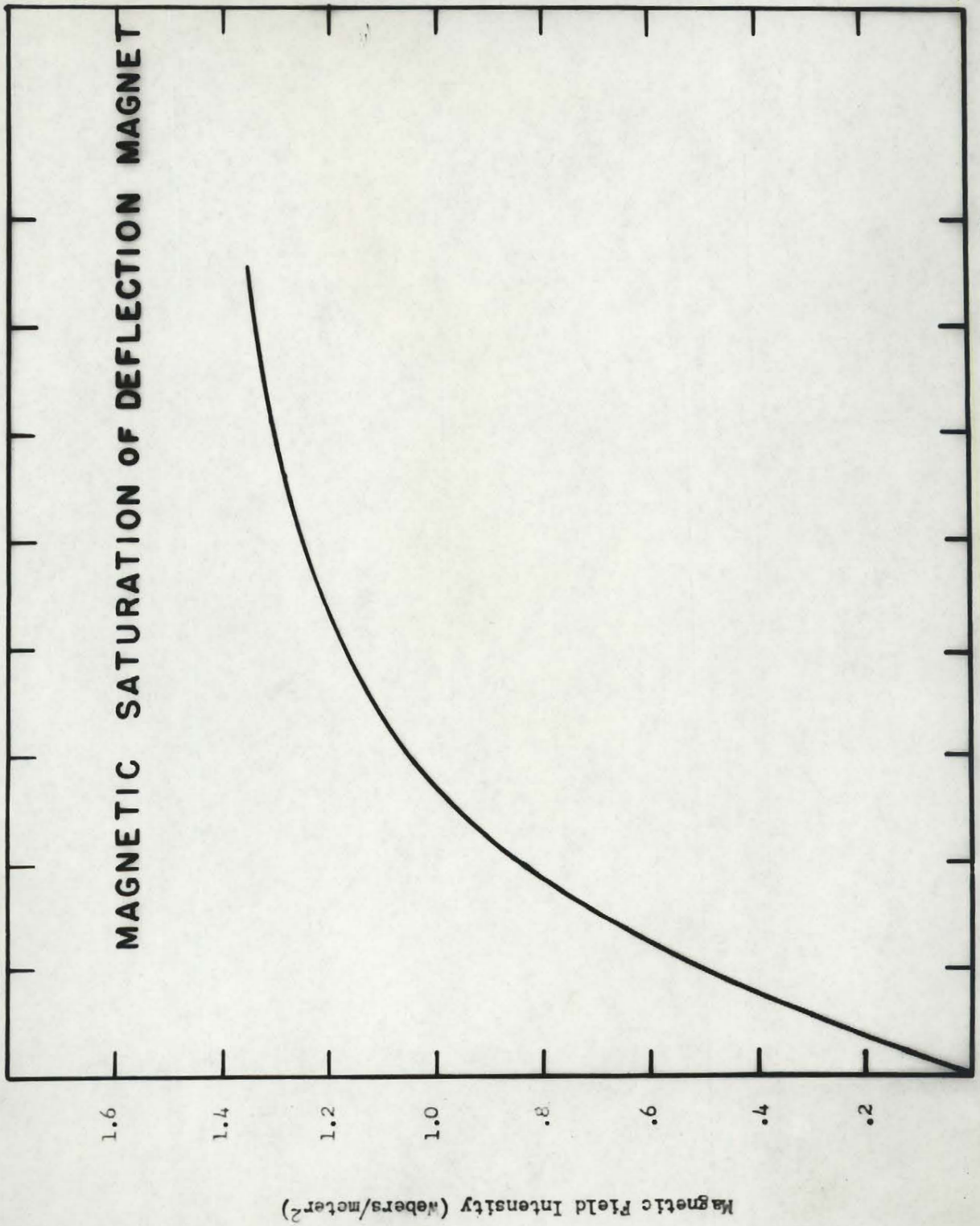
MAGNETIC SATURATION OF DEFLECTION MAGNET
Magnetic Field Intensity (webers/meter²)
1.6
1.4
1.2
1.0
.8
.6
.4
.2
10
20
30
40
50
60
70
80
Magnet Current (Amperes)

Fig.24.

follows:

(i) The current decrease due to an increase in resistance of the coil of 20 per cent brought about by a 50°C temperature rise.

(ii) A fluctuation of 1 per cent in the frequency with a corresponding change in the output voltage.

(iii) A shift in the mains voltage on the driving motor of up to 20 per cent. This will cause the generator output to change by less than 3 per cent.

(iv) The motor generator ripple and brush noise were detected on an oscilloscope. A 0.1 volt ripple at 60 cycles, and 0.05 volts of high frequency brush noise were observed. Because of the high reactance of the magnet coil, these will produce a negligible fluctuation on the output current.

The total possible current fluctuation is therefore less than 25 per cent.

(b) General Discussion of Magnet Regulation Systems

Three suitable types of regulation were investigated. These are based on control by the magnet current, the beam position, or the magnetic field.

A proton resonance magnetic field control[19] has been used to give a regulation factor of 4×10^4. This set up is somewhat more complex than the necessary regulation factor of 1000 demands.

A control based on the beam position is perhaps the most realistic approach, since it would compensate for any changes in

the primary beam energy or position as well as for shifts in the field of the magnet. This system depends on a fairly reliable, steady external beam, so it was temporarily abandoned until such a beam was obtained. The magnet current stabilization, which appears to be the simplest and most reliable method of field control, was chosen as the regulation system. Such a circuit could be converted with a minimum of change to a beam position regulator.

(c) Current Regulator

A block diagram of the current regulator is given in Fig. 25 A voltage signal, proportional to the current, is fed from the series shunt to a "chopper" or "converter". This converter compares the shunt signal with a variable reference voltage, the output being a 60 cycle square-wave proportional to their difference in potential. This square wave is greatly amplified, then rectified in a phase sensitive detector (Ø.S.D.). The polarity of the output of the detector depends upon the phase of the input error signal. At this point the error signal is mixed with a signal proportional to the rate of change of the generator voltage. This differential signal prevents "hunting" of the generator and acts as a feedback loop for the higher frequency components of the generator voltage fluctuations. The resultant signal is amplified in a D.C. coupled network whose output is fed onto the grids of six parallel-connected 6AS7's arranged to control the shunt field current of the generator.

In such a degenerate type regulator, the fluctuations in the output current are reduced by the smoothing factor

BLOCK DIAGRAM OF MAGNET CURRENT REGULATOR

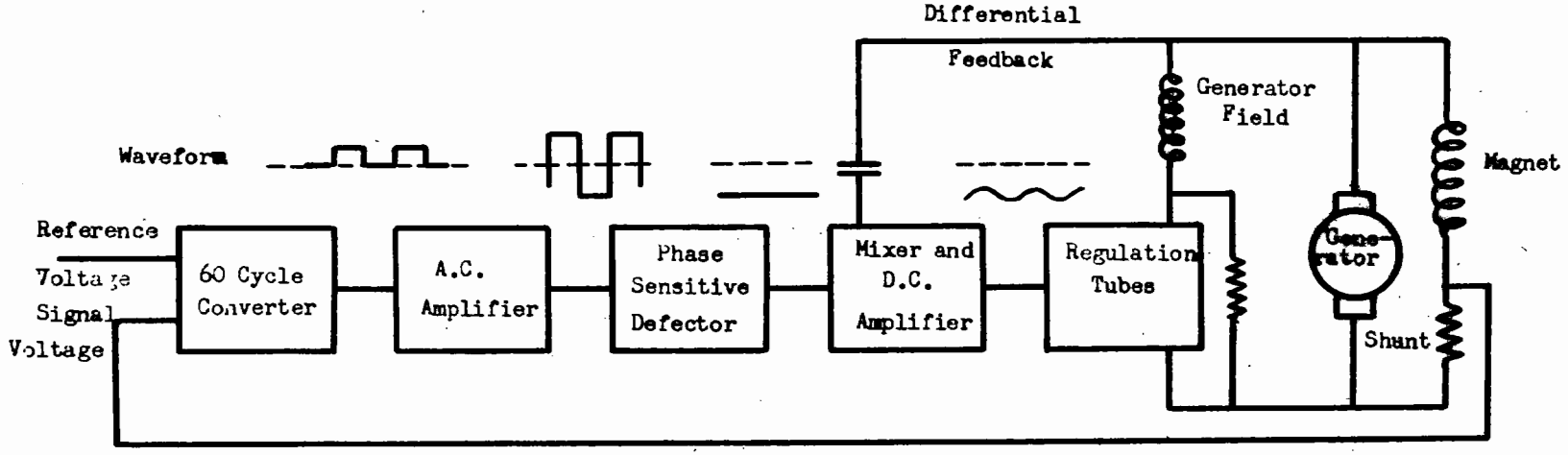

Fig.25.

$$\alpha = \frac{1}{1 + \beta A}$$

where A is the overall gain and β is the feedback ratio. The product βA is known as the loop gain of the system. In order to keep the current fluctuations less than 0.1 per cent with a possible variation of 25 per cent when no regulation is used, a loop gain of 250 is necessary.

Stability is often a problem in a high gain feedback circuit, particularly in the high and low frequency cutoff regions. Oscillations may result from large phase shifts in the amplifier or motor generator. For simple systems, the stability problem may be easily analysed on the basis of the asymptotic frequency response of the circuit. A general criterion for stability is that when the loop gain drops to unity, the response should be decreasing with a slope of less than 12 decibels/octave. In order to avoid oscillations, the time constants, gains, and mixing frequencies of the circuit must be suitably adjusted.

The details of the circuit are shown in Fig. 26. The regulation signal is taken from a 50 millivolt (at 75 amperes) shunt so the feedback factor β is approximately 5×10^{-4}. This signal is compared with the reference voltage supplied by a 5651 regulator tube. In a two hour test this voltage showed less than 0.02 per cent drift. Three 62J7's amplify the signal by a factor of over 10^4. In order to eliminate 60 cycle pickup from the filaments of the first tube, they are heated from a 6 volt D.C. power supply.

MAGNET CURRENT REGULATOR

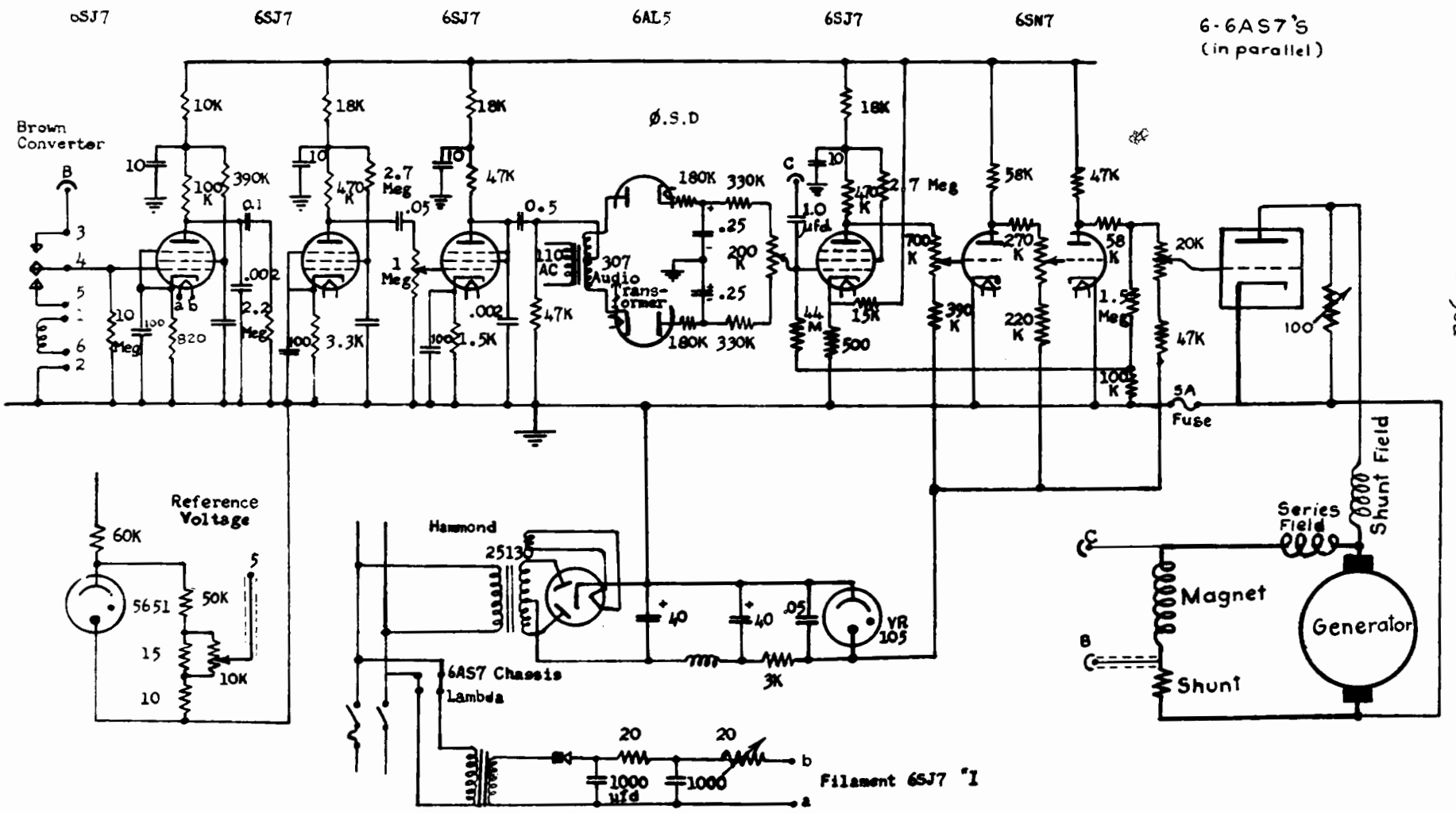

Fig.26.

The phase sensitive detector is of somewhat unconventional design, the only transformer needed being one to produce the comparison 60 cycle. The 47 K resistor at the input to the detector is chosen such that the time constant associated with it is short compared to the filtering time constant of the detector. If this is not achieved, the gain of the detector is seriously reduced. The filtering network following the detector has a cut-off frequency of 2 cycles/sec, which partially limits the band width of the current-feedback loop.

The current-feedback and voltage-feedback signals are mixed in an R-C circuit following the phase sensitive detector. The mixer crosses over from one signal to the other at a frequency of 0.8 cycles/second. The resultant signal is amplified by a factor of 1000 in the direct coupled D.C. amplifier. The gain and D.C. levels are stabilized by 0.1 per cent inverse feedback from the plate of the 6SN7 to the grid of the previous 6SJ7. The D.C. levels are so adjusted that the grids of the 6AS7's may be driven 60 volts negative and only a few volts positive.

The 6AS7's and motor generator form the next unit in the circuit, with a combined gain of about 3 and a cut-off frequency of 0.3 cycles /second. The magnet itself has a time constant of 4 seconds (f_c = 0.25 cycles/second) which cuts off the response of the current-feedback loop at a very low frequency and produces a large phase shift in the circuit. The voltage-feedback loop is independent of the time constant of the magnet, so it greatly improves the stability of the

regulator. The asymptotic loop frequency response of the circuit as seen at the mixer is shown in Fig. 27. The current-feedback loop gain at zero frequency of 1.5×10^4 and the voltage-feedback loop gain of 3×10^3 are balanced so that the combined asymptotic slope increases to 12 dedibels/octave for only a very short frequency range. The resultant stability of the system should be good.

The tap on the 100 ohm generator-field shunt-resistor is adjusted to the point where 120 volts are generated when the bias on the 6SJ7's is 0 volts. The circuit will then regulate in the range from 40 to 65 amps. The magnet and the cathodes of the 6AS7's are grounded through a 5 ampere fuse. This protects the system in case a short were to develop in the magnet coil.

The whole unit is mounted on the magnet base close to the signal lead from the shunt, so noise pickup is minimized. The helipot reference voltage adjustment may be adjusted from the control desk by means of a pair of selsyns.

4. Control and Protection Circuitry of Magnet

The control circuits for the magnet and associated equipment are given in Fig. 28. Dual control is provided so the magnet may be operated from the cyclotron room, or from the main control panel. A wheatstone bridge type circuit is employed so that the neon lights for the water flow gauge will be extinguished when the wire contact and mercury column are separated by a column of water whose resistance is over 30 K ohms.

ASYMPTOTIC RESPONSE OF MAGNET CURRENT REGULATOR

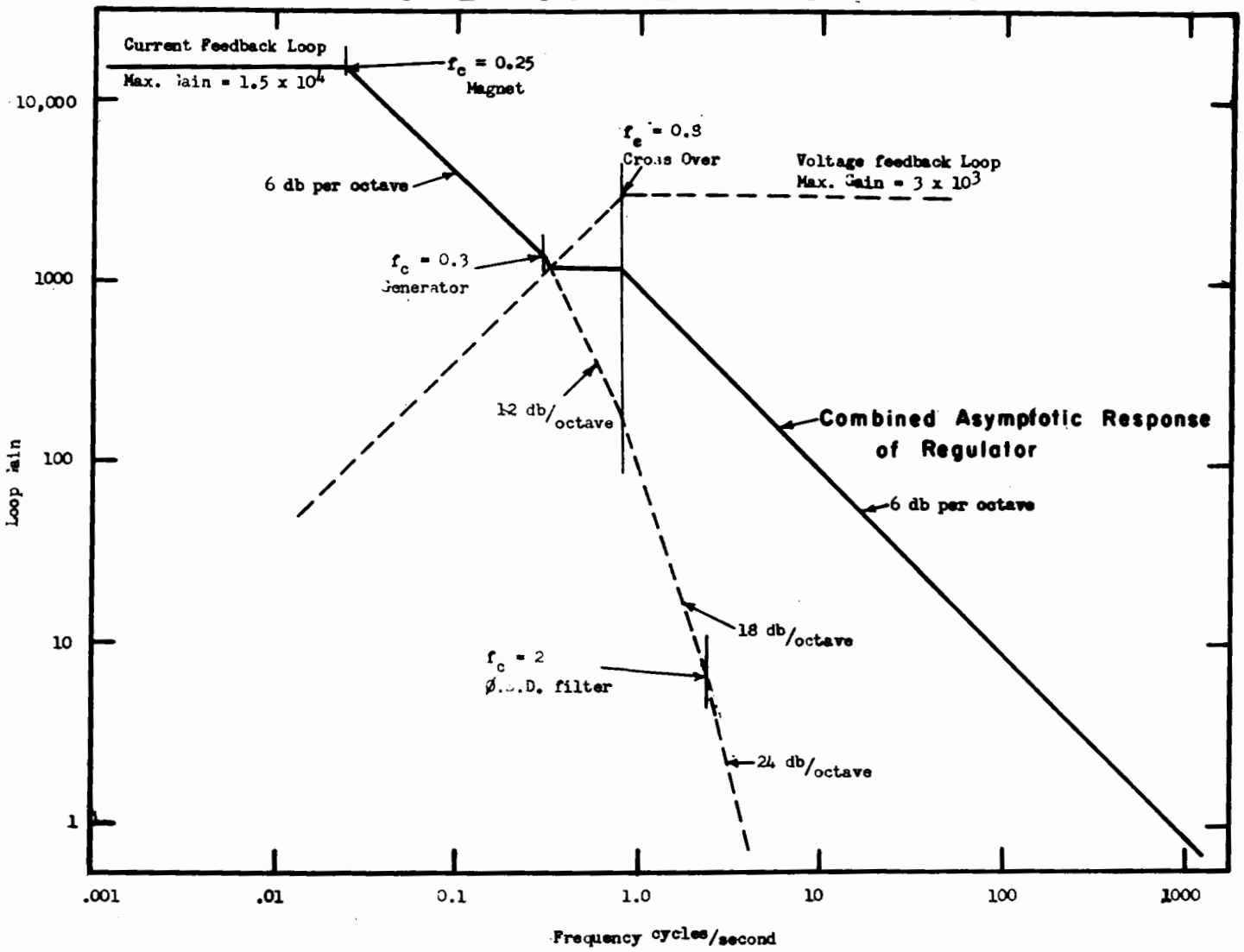

Fig.27.

DEFLECTION MAGNET CONTROLS

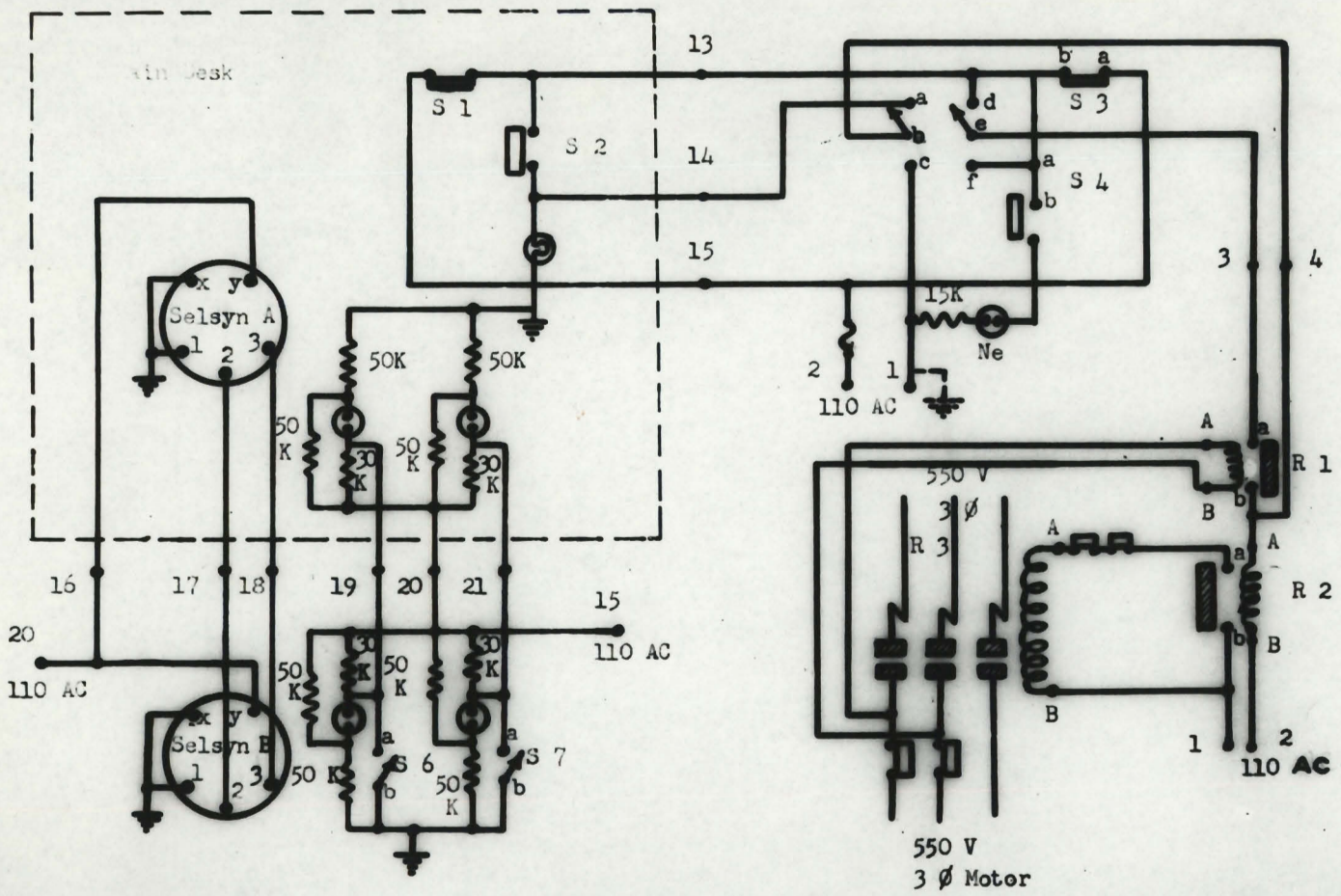

S 1, S 3 - Generator off
S 2, S 4 - Generator on
S 5 - Control transfer
S 6, S 7 - Bernouli gauge Mercury switches

R 1 - Hold on Relay (550 AC)
R 2 - Preliminary Relay (110 AC)
R 3 - Contactor (110 AC)

• numbers correspond to terminal strip connections

Fig.28.

E. External Beam in Corridor

(1) Shielding

The deflection magnet bends the beam into a 24" wide by 8" deep steel casing which was pushed through a tunnel dug in the 11 ft shielding wall between the cyclotron room and the corridor (Fig.1). The voids about this casing were filled in by blowing a liquid cement mixture into the cavities. It is planned to fill the inside of the casing with concrete blocks fitted about the proton pipe if further shielding is necessary.

Measurements in the corridor with a slow neutron counter show that most of the observed 1500 cm^2/sec flux of slow neutrons enters through the doorway into the cyclotron room; in fact, the intensity decreases inside the hole. If an improvement in the low energy neutron background is desired for subsequent experiments, a concrete and cadmium door may have to be installed in the entrance corridor.

A very important shielding problem appears to arise in the "disposal" of the protons after they pass through the target. A test run was made with the beam being stopped in a 6" deep lead cylinder with 4" thick walls. A $1\frac{1}{2}$" x $1\frac{1}{2}$" NaI scintillation counter placed 3 feet from the cylinder and shielded by 4" more lead shows a background of 200 counts/second above 8 Mev for an internal cyclotron beam of 1μa; this must be greatly reduced. It has been suggested that the beam be stopped in a hole drilled to a depth of several feet in the opposite wall of the corridor. Some replaceable target in which the protons produce little activity (i.e. Co) could serve as the

"sink" for the proton beam.

(2) Deflection of the Beam

The magnet was aligned with the help of X-ray plates taken at the end of the proton pipe in the cyclotron room, and at the exit from the magnet. From the shadow of a heavy cross of metal at the entrance to the magnet, the magnet current needed to bring the beam centrally through the pole-pieces was found to be 55 amperes. When the magnet was properly orientated, a well-focused beam $\frac{1}{4}$" high and $2\frac{1}{2}$" wide was observed out in the corridor. The beam intensity is 0.82×10^{-11} amperes passing through the $\frac{7}{8}$" aperture of the Faraday cup with a $.5 \times 10^{-6}$ ampere internal cyclotron beam. The total external beam at this point is estimated to be 2×10^{-11} amperes so the overall extraction efficiency is 4×10^{-5}, a factor of 3 less than the maximum theoretical efficiency.

(3) Energy Measurement of the Proton Beam

The energy of the proton beam was determined from its range in aluminum. The absorbers consist of a heavy aluminum block, 6.4580 gms/cm^2 thick, and 7 thinner foils mounted on two concentric wheels which give a total of 12 absorber thicknesses. The foil wheels were turned remotely through a selsyn motor and geared chain drive.

A proton detector employing a 1" x 1" NaI (Th) crystal spectrometer behind the absorber wheels was employed instead of the Faraday cup. In order to keep the counting rate low enough so that "pile up" did not occur in the scintillation counter, it was necessary to run the

cyclotron with the ion source and hydrogen supply off. It was found that for counting rates faster than 100/second, considerable pile up of pulses occurs. This was confirmed by observing the photomultiplier pulses in a cathode ray oscilloscope and by integral bias counting.

Two methods of monitoring the beam were employed, both of which appeared satisfactory. In the first method, the main absorber had a $\frac{3}{16}$" hole drilled through it to pass high energy protons. Both the absorbed beam and the monitor beam fell on the centre of the NaI crystal. These monitor protons were counted in a separate scaler whose bias was set above the maximum energy of the protons passing through the absorbers. To minimize the effects of degraded, slit scattered protons from the small aperture hole, the acceptance bias of the monitor was varied in accordance with the maximum energy of the protons passing through the foils. (Fig. 29)

A second monitoring system made use of a separate stilbene crystal and RCA 5819 photomultiplier mounted behind and just above the $\frac{1}{2}$" diameter hole in the brass collimator. The first run was made with defining baffles, which gave a theoretical energy resolution of better than 1 per cent at the target and so served as a check of the measurement system. For the second run, the baffles were removed, and slightly higher energy protons obtained by increasing the deflection magnet current. The following table summarizes the experimental conditions.

FOIL WHEEL DETERMINATION OF PROTON ENERGY SPECTRUM.

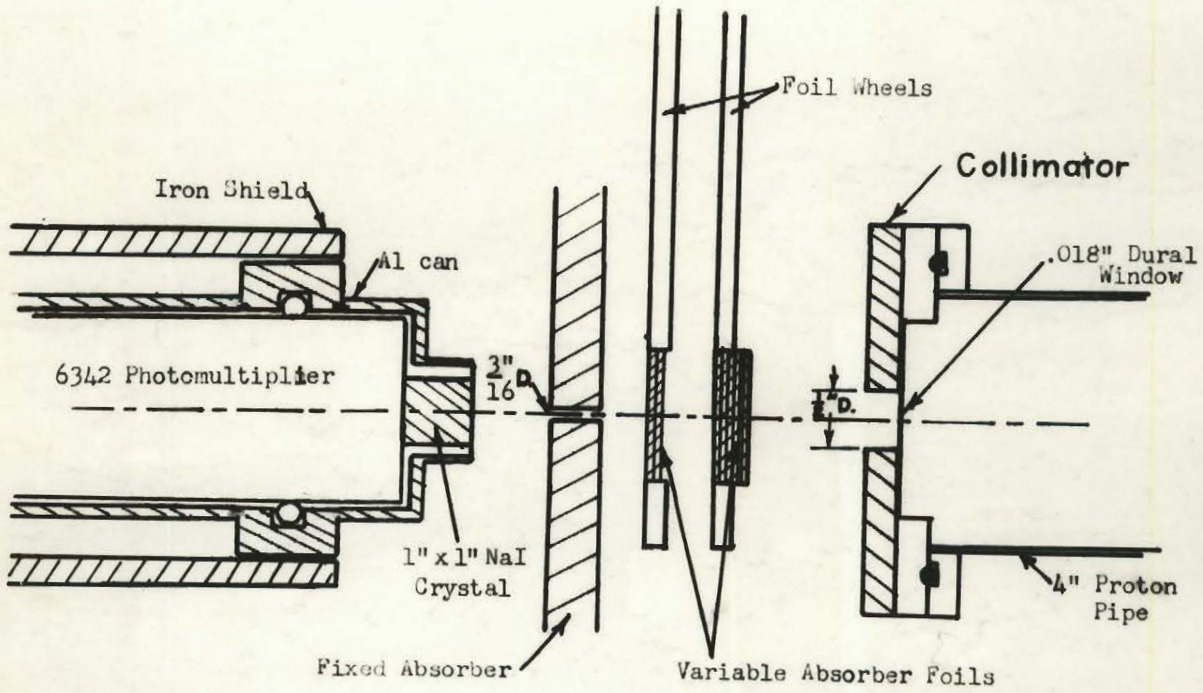

Fig.29.

Table II

Cyclotron	Ion source and H_2 off Oscillator - 6.5 Kv Bias - 1000 volts.	same
Baffles and collimation	$\frac{1}{4}$" slit at exit from cyclotron $\frac{3}{4}$" diameter collimator at entrance of steering magnet	No baffles $\frac{1}{2}$" diameter collimator 4" from crystal
	$\frac{1}{2}$" diameter collimator approximately 8" from NaI crystal.	
Monitor	High energy protons passing through $\frac{3}{16}$" hole in absorbing block.	Stilbene crystal scintillation counter mounted just above beam
Steering Magnet current	47 amperes	50 amperes

The beam intensity fluctuated by a factor of 2 or more during a one minute run, and its position shifted slightly with a resultant change in the relation between the monitor and the counter. By taking the average of several determinations, it was possible to reduce the probable error in individual points to $\pm$ 4 per cent.

The proton energies were calculated from the range-energy curves of W. A. Aron et al,[20] which agree with experimental observations to $\pm \frac{1}{2}$ per cent.[21] The accuracy of the mean proton energy determination is thus limited to the 1.5 Mev energy resolution of the absorbers. The measured energy distributions are shown in Fig.30 in solid lines. The energy straggle in the absorbers corresponds to a gaussian distribution with full-width at half maximum of 1.5 per cent.

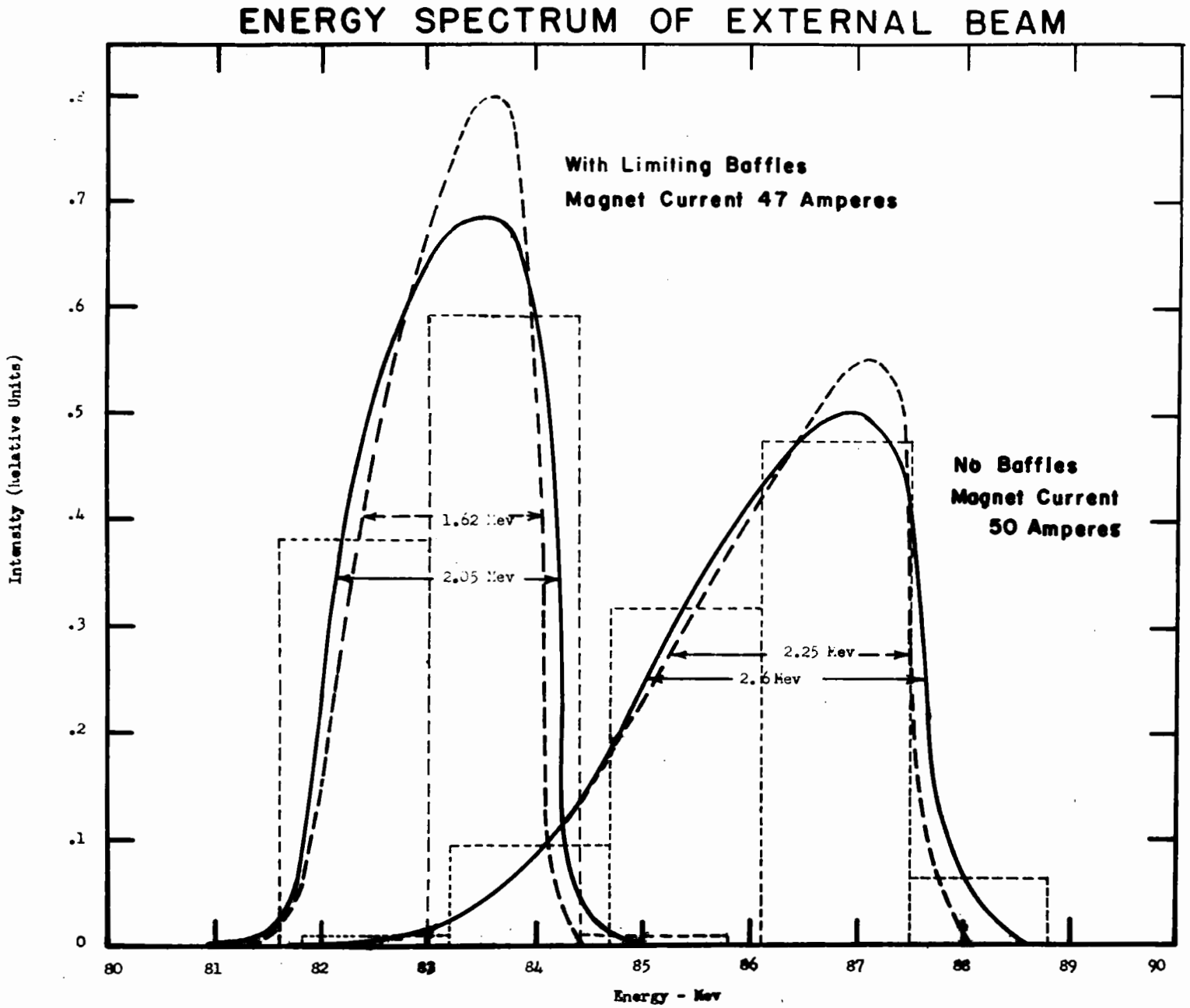
ENERGY SPECTRUM OF EXTERNAL BEAM
With Limiting Baffles
Magnet Current 47 Amperes
No Baffles
Magnet Current
50 Amperes
1.62 Kev
2.05 Kev
2.25 Kev
2.6 Kev
Intensity (Relative Units)
Energy - Kev
0
.1
.2
.3
.4
.5
.6
.7
80
81
82
83
84
85
86
87
88
89
90

Fig.30.

Using the approximation that the energy spectrum is gaussian, the approximate corrected distributions (dashed lines) were drawn.

From the magnetization curve for the deflection magnet, the change in the mean energy between two runs may be 3.8 ± .5 Mev. The measured difference is 3.6 ± .2 Mev. Because the energy resolution due to the minimum foil thickness is 1.5 Mev, the indicated 1.62 Mev full energy width at half maximum for the first spectrum is probably too large.

(4) Burst Length of Beam

The burst length of the beam was measured by observing the fluorescence of a zinc sulphide screen by means of a photomultiplier and oscilloscope. The response of the photomultiplier circuit was checked by allowing the photomultiplier to observe a 50 μ sec portion of a sweep on a Techtronix scope with a fast (approx 10 μ sec) blue screen. The pulse was square to within the decay time of the screen. The zinc sulphide screen also has a decay time of approximately 10 μ seconds.

The burst appeared to be roughly gaussian in shape and of 30 μ seconds full width at half maximum. The length of the burst is independent of most cyclotron operating parameters, including even the ion source pulse length. Detuning the cyclotron in any way only decreases the pulse intensity, and makes the intensity vary erratically. Slow fluctuations with a period of several seconds also occur.

This short pulse length is of particular importance for any experiments where the measurement of high counting rates are necessary. The repetition rate of the cyclotron is 200 bursts per second, so most of the counts are concentrated in 6×10^{-3} seconds. For an average counting rate of 200 counts per second, the instantaneous counting rate for the detection equipment is 33,000 counts per second, which will necessitate a fairly large dead-time correction for most scaling equipment.

The double (or higher) piling of pulses in the counter may be of great importance, especially if one is observing a small high energy counting rate and discriminating against an intense background of lower pulses. The piling of pulses is given approximately by

$$(N_{av}^{(x)}) = N^x (\Delta t)^{x-1} \times 6 \times 10^{-3}$$

where x is the number of pulses piled up, N is the instantaneous counting rate, and Δt is the length of the photomultiplier pulse. For an average counting rate of 200 counts per second, the double piling of pulses is 6/second or 3 per cent of the gross counting rate. This effect was observed during the measurement of the energy of the beam. It was reduced by shortening the pulse length, and reducing the cyclotron output until the average counting rate was less than 100 per second.

SUMMARY

An external proton beam from the McGill synchro-cyclotron has been obtained. A coulomb scatterer and magnetically shielded channel was employed to extract a portion of the internal beam. The extracted beam is deflected through a shielding wall into a low background region.

A general shimming of the cyclotron was undertaken to centre the internal beam in the cyclotron to prevent its premature blowup. The field was shimmed to within $\pm$ 10 gauss from the mean at any given radius.

An extraction system consisting of a 1.4 gm/cm^2 uranium scattering target followed by a magnetic shielding channel was designed and constructed. It was installed in the cyclotron and aligned by the current-carrying stretched wire technique. Perturbations in the field due to the channel were shimmed out to within $\pm$ 30 gauss from the mean at a radius of 36". The system accepts protons which are scattered outward through 5.5° by the uranium target positioned 34° in azimuth before the magnetic channel. These are close to the optimum conditions for coulomb scattering extraction from this cyclotron.

An electrometer tube direct current amplifier was designed and constructed in order to measure the external proton current.

After considerable adjustment, a satisfactory beam of $8.7 \pm 1.5 \times 10^{-11}$ amperes per microamp of internal beam was obtained at the exit port from the cyclotron. This beam was highly divergent in both the horizontal and vertical phases. Measurements showed

that the beam was being overfocused vertically and defocused horizontally by the fringing fields in the cyclotron. A series of iron wedges was installed inside the cyclotron to produce positive lateral field gradients along the path of the beam. With these, a beam is obtained which is slightly convergent in the vertical plane and divergent in the horizontal. This beam is $\frac{1}{4}$" high and 3" wide at the entrance to the deflection magnet. The extracted beam at this point is $4.3 \pm .9 \times 10^{-11}$ amperes as measured by a Faraday cup.

A large double focusing deflection magnet was built to bend the proton beam and direct it through an 11 foot thick shielding wall into the cyclotron corridor. This magnet focuses monoenergetic protons in both the horizontal and vertical planes onto a target placed in the corridor. It also disperses the beam horizontally with a resolution of 2 Mev per inch. The magnet field is regulated to within 1 part in 1000 by a feedback circuit which controls the current in the magnet.

The external proton beam was bent through a hole in the 11 foot cyclotron shielding wall into the entrance corridor. A beam of $4 \pm 1 \times 10^{-11}$ amperes per microamp of internal cyclotron beam was obtained over an area $\frac{1}{4}$" high and $2\frac{1}{2}$" wide. This compares favourably with the maximum theoretical extraction efficiency of 13×10^{-11} amperes per microamp of internal beam.

The beam energy is 87 Mev measured from its range in aluminum. The energy spectrum through a $\frac{1}{2}$" collimator has a width of 2.2 Mev at half maximum.

Preliminary background measurements show that the unused portion of the proton beam will excite a large background during a run unless the beam is disposed of in some better manner. The external beam pulse was found to be only 30 μ seconds in duration. To prevent an appreciable piling up of pulses in the counting system, average counting rates much higher than 100 per second must not be used in external beam experiments involving the instantaneous counting of events.

APPENDIX

(a) Figure 21(a) shows the general paths for particles moving from a point source in a horizontal plane. The notation is that of Cross(16).

Let A H K B be the path of a mean particle of momentum P_o and $A'H'K'B'$, the path of a particle differing in initial lateral position s and direction α from that of the mean particle.

After it has left the magnetic field, the lateral displacement x from the central path is, according to Cartan [22],

$$x = \alpha\left[\frac{(1 - pq)\cos\epsilon_1 \cos\epsilon_2}{\sin\Omega}\right] - s\left[q\frac{\cos\epsilon_2}{\cos\epsilon_1}\right] \qquad (1)$$

where

$$p \equiv \frac{l' \sin\Omega}{\cos^2\epsilon_1} - \frac{\cos(\phi - \epsilon_2)}{\cos\epsilon_1}$$

$$q \equiv \frac{l'' \sin\Omega}{\cos^2\epsilon_2} - \frac{\cos(\phi - \epsilon_1)}{\cos\epsilon_2} \qquad (2)$$

$$\Omega = \phi - \epsilon_1 - \epsilon_2$$

Note that the distances are given in units of the radius of curvature, i.e. $\rho = 1$.

The vertical focusing is illustrated in Figure 21(b). The distance y from the median plane is given by [23]

$$y = y_o\left[1 - \phi\tan\epsilon_1 - l_v''\{\tan\epsilon_1 + (1 - \phi\tan\epsilon_1)\tan\epsilon_2\}\right]$$

$$+ \omega\left[\phi + l_v'(1 - \phi\tan\epsilon_2) - l_v' l_v''(\tan\epsilon_1 + (1 - \phi\tan\epsilon_1)\tan\epsilon_2) + l_v''(1 - \phi\tan\epsilon_2)\right]$$

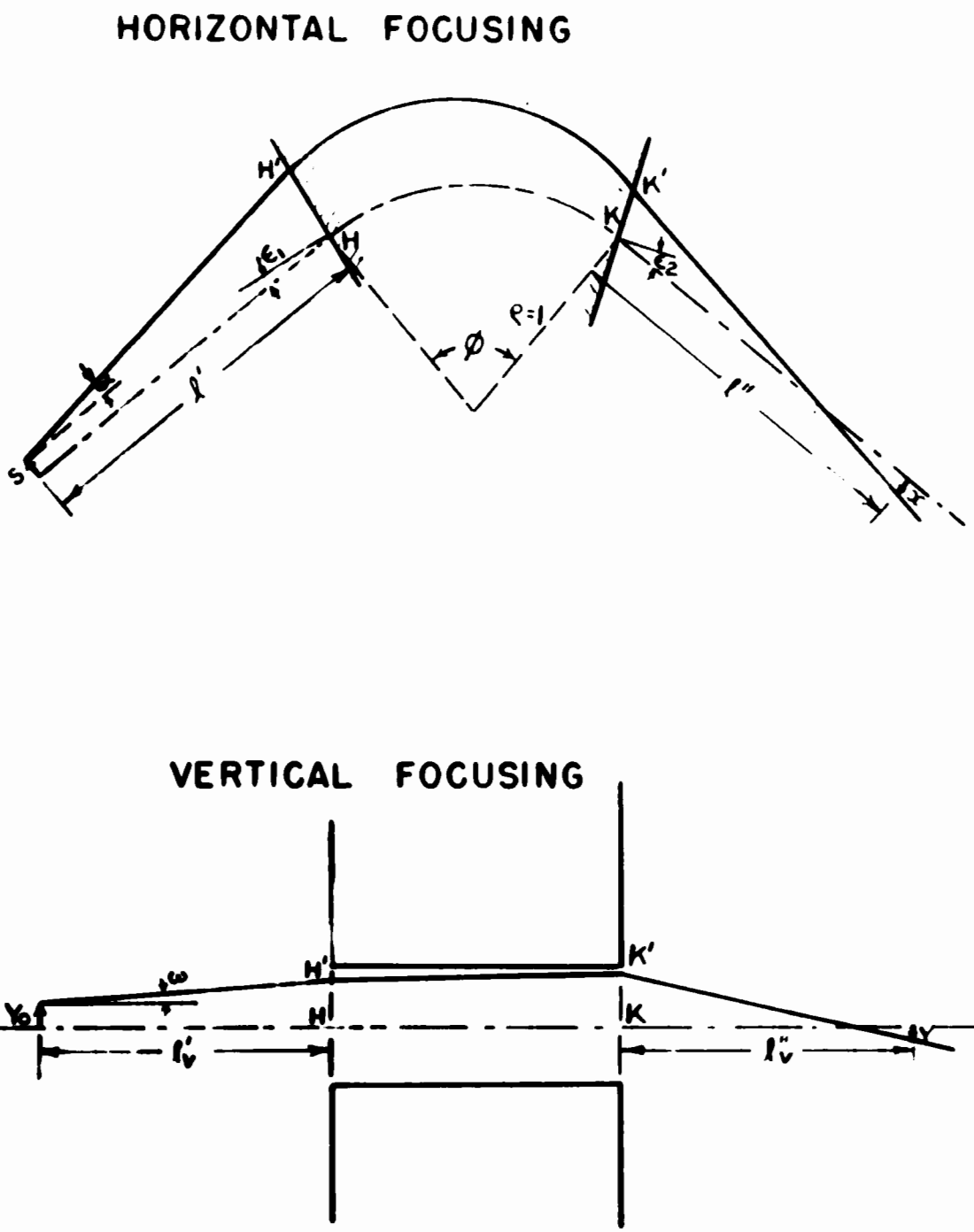
HORIZONTAL FOCUSING
H'
K'
K
H
ε1
ε2
ρ=1
φ
l'
l''
S
VERTICAL FOCUSING
K'
H'
ω
H
K
Y0
l'v
l''v
Y

Fig.31.

A focusing effect is produced by positive angles ϵ_1 or ϵ_2, defocusing by negative angles.

Horizontal focusing occurs (the coefficient of α in equation 1 vanishes) when 1'' takes the value:

$$1'' = \cos\epsilon_2 \; \frac{\sin\phi + \left\{1' \frac{\cos(\phi - \epsilon_1)}{\cos\epsilon_1}\right\}}{1' \frac{\sin\Omega}{\cos\epsilon_1} - \cos(\phi - \epsilon_2)} \tag{3}$$

Similarly, vertical focusing occurs when the coefficients of ω vanish.

$$1_v'' = \frac{\phi + 1_v'(1 - \phi\tan\epsilon_1)}{1_v'\left[\tan\epsilon_1 + (1 - \phi\tan\epsilon_1)\tan\epsilon_2\right] - (1 - \phi\tan\epsilon_2)} \tag{4}$$

One may put equations (3) and (4) in the forms

$$\frac{1}{1''} = \tan(\phi - \psi) - \tan\epsilon_2 \tag{5}$$

$$\frac{1}{1_v''} = \tan(\epsilon_2) - \left(\frac{1}{\phi - \cot\eta}\right) \tag{6}$$

where ψ and η are defined as

$$\tan\psi = \tan\epsilon_1 + \frac{1}{1'} \tag{7}$$

$$\tan\eta = \tan\epsilon_1 - \frac{1}{1_v'} \tag{8}$$

The double focusing from a point source into a point image occurs when

$$1' = 1_v'$$

$$1'' = 1_v'' = 1_d''$$

Then one may obtain the following relations between the focal lengths and the angles of the sector.

$$\tan \epsilon_2 = \tfrac{1}{2}\left[\tan(\phi - \psi) + \frac{1}{(\phi - \cot\eta)}\right] \qquad (9)$$

$$\frac{1}{l_d''} = \tfrac{1}{2}\left[\tan(\phi - \psi) - \frac{1}{(\phi - \cot\eta)}\right] . \qquad (10)$$

The case in which the object and image distances are fixed, with the angles ϵ_1 and ϵ_2 as variables, has no direct algebraic solution. It is easily solved graphically, or by the method of successive approximations.

(b) Energy Resolution of Magnet

Protons with moments p_o and p' enter the magnet at the same position and are bent with radius of curvature ρ_o and ρ'. At a distance l'' from the exit of the magnet they are separated by the lateral distance x given by

$$x = x_K + (\phi_o - \phi')\left\{l'' + d\rho(1 - \cos\phi_o)(\tan\epsilon_2)\right\} \qquad (11)$$

where $d\rho = \rho' - \rho_o << \rho_o$.

The path length d' is related to the radius of curvature ρ' by

$$d' \cong \phi\rho'\left(1 + \frac{d\rho}{\rho}\sin\phi\right) - d\rho\,(1 - \cos\phi)\tan\epsilon_2 \qquad (12)$$

and

$$d' = \phi'\rho' . \qquad (13)$$

Substituting for ϕ' in Equation (11),

$$x \cong \frac{d\rho}{\rho}\left\{(\rho - l''\tan\epsilon_2)(1 - \cos\phi) + l''\sin\phi\right\} . \qquad (14)$$

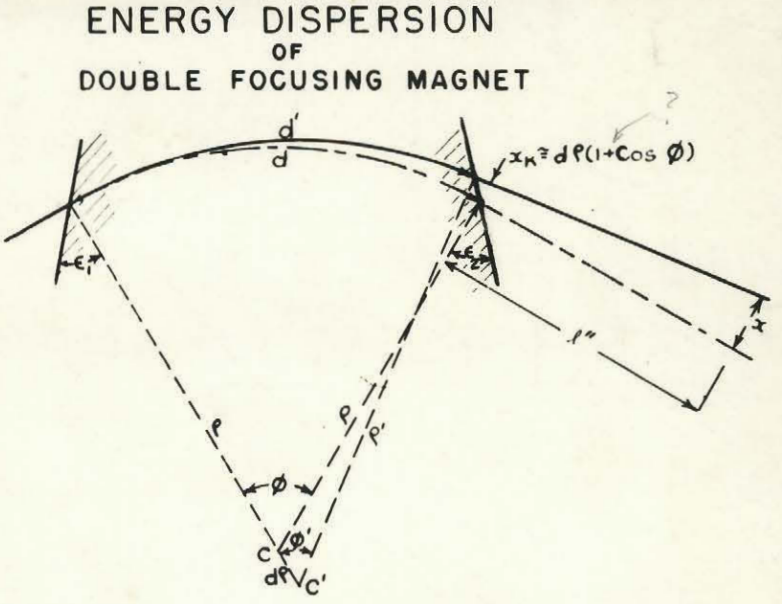
ENERGY DISPERSION
OF
DOUBLE FOCUSING MAGNET
d'
d
$x_K = d\rho(1+\cos\phi)$
ϵ_1
ϵ_2
x
l''
ρ
ρ
ρ'
ϕ
C
ϕ'
$d\rho$
C'

Fig.32.

References

1. S. Fernbach, R. Serber, T.B. Taylor. Phys.Rev. 75, 1352 (1949).
2. E. Fermi. Nuovo C.mento (9) 11, 407 (1954).
3. J.L. Tuck and L.C. Teng. Institute of Nuclear Studies. Progress Report (Univ. of Chicago) Chapter VIII (1950).
4. J.L. Tuck and L.C. Teng. Phys.Rev. 81, 305 (1951).
5. A.V. Crewe and K.J. LeCouteur. Rev.Sci.Inst. 26, 725 (1955).
6. D.W. Hone. Unpublished Thesis, McGill University (1951).
7. J.S. Kirkaldy. Unpublished Thesis, McGill University (1953).
8. J.S. Kirkaldy. McGill Radiation Lab. Report (May 1954).
9. J.D. Prentice. Unpublished Thesis, McGill University (1953).
10. H. Moody. Unpublished Thesis, McGill University (1955).
11. R.L. Aamodt, V. Peterson, R. Phillips. UCRL 1400 (September 1951).
12. K. Siegbahn. "Beta and Gamma Ray Spectroscopy", North Holland Pub.Co.
13. H.S. Snyder and W.J. Scott. Phys.Rev. 76, 220 (1949).
14. N.M. Hintz and N.F. Ramsey. Phys.Rev. 88, 19 (1952).
15. W.E. Crandall, G.P. Millburn, R.V.Pyle, and W. Birnbaum. UCRL 2566 (1955).
16. H.M. Skarsgard. Unpublished Thesis, McGill University (1955).
17. M. Camac. Rev.Sci.Inst. 22, 197 (1951).
18. W.G. Cross. Rev.Sci.Inst. 22, 717 (1951).
19. H.A. Thomas. Electronics 25, 114 (January 1952).
20. W.A. Aron, B.G. Hoffman, F.C. Williams. AECU 663.
21. N. Bloemberger and P.J. Van Heerden. Phys.Rev. 83, 583 (1951).
22. L. Cartan. J.Phys. et Radium 8, 453 (1937).
23. M. Cotte. Annales de Physique 10, 333 (1938).